

SLOVAK UNIVERSITY OF TECHNOLOGY IN BRATISLAVA  
Faculty of Chemical and Food Technology  
Institute of Information Engineering, Automation, and Mathematics  
Radlinského 9, 812 37 Bratislava

---



# Nonlinear Model Predictive Control of a Diesel Engine with Exhaust Gas Recirculation and Variable Geometry Turbocharger

Diploma thesis

Martin Herceg

**supervisors:**

Dipl.-Ing. Tobias Raff

Dr.-Ing. Rolf Findeisen

Doc. Dr.-Ing. Miroslav Fikar

Bratislava, 2006

# Acknowledgement

The diploma thesis was written during my stay at Institute for Systems Theory and Automatic Control (IST), University of Stuttgart, supported under the European SOCRATES/ERASMUS exchange program. The cooperation between the Institute of Information Engineering, Automation, and Mathematics (IIEAM), Slovak University of Technology in Bratislava and the IST would not have been established without help of several people.

Firstly my thanks goes to Doc. Dr.–Ing. Miroslav Fikar, head of the IIEAM, for initial arrangement of my stay and for his support, encouragement and advices given throughout my studies. Secondly I am very grateful to Prof. Dr.–Ing. Frank Allgöwer, head of the IST, for financial support and for introducing me into the research group at IST.

Many thanks go to my supervisors at IST, namely Dipl.–Ing. Tobias Raff and Dr.–Ing. Rolf Findeisen, for helping me with understanding NMPC problematics and for their fruitful discussions. I do not want to forget Dr.–Ing. Christian Ebenbauer who was always willing to help me with any kind of problems.

Last but not least I want to express my thanks to Doris Köhler, for her help with the paper work, to every member member of IST and IIEAM, and finally to my family for their understaning and support from the beginning of my university studies.

Martin Herceg

Stuttgart, May 22, 2006

# Abstract

The presented work deals with the control of a diesel engine, equipped with a variable turbocharger coupled with an exhaust gas recirculation valve. In contrast to existing control approaches in the literature, nonlinear model predictive control (NMPC) is used to control a diesel engine. The reason for applying NMPC comes from the ability to consider directly constraints of the control problem and to use a nonlinear model to improve performance. The performance of NMPC controller is compared with a linear-quadratic regulator (LQR) and a controller based on the input-output linearization method. With this in mind, the goal of the diploma thesis is to show that NMPC can be considered as a benchmark for other control methods.

# Abstrakt

Diplomová práca sa zaoberá problémom riadenia vznetrového motora vybaveného turbokompresorom s variabilnou geometriou lopatiek a ventilom na recirkuláciou časti spálenej zmesi metódou nelineárneho prediktívneho riadenia. Nelineárne prediktívne riadenie je optimálne založený spôsob riadenia, ktorý priamo využíva model vznetrového motora a zároveň umožňuje prihliadať na pracovné obmedzenia. Cieľom diplomovej práce je prezentovať možné optimálne riešenia pre vznetrový motor, ktoré možno považovať ako určité meradlo pre ostatné metódy. S týmto zámerom sa výsledky porovnávajú s optimálnym kvadraticko-lineárnym riadením a metódou založenou na vstupno-výstupnej linearizácii.

# Contents

<b>1</b>	<b>Introduction</b>	<b>1</b>
<b>2</b>	<b>Control Problem</b>	<b>3</b>
2.1	Principle of EGR and VGT in Diesel Engine . . . . .	3
2.2	Control Problem Formulation . . . . .	4
2.3	Signal Overview . . . . .	6
<b>3</b>	<b>Model of a Diesel Engine</b>	<b>8</b>
3.1	Physical Model . . . . .	8
3.2	Control Model . . . . .	12
<b>4</b>	<b>Nonlinear Model Predictive Control</b>	<b>15</b>
4.1	NMPC Setup . . . . .	15
4.2	Quasi-Infinite Horizon NMPC Scheme . . . . .	16
4.3	Computation of the Terminal Region . . . . .	18
4.4	NMPC Implementation . . . . .	20
<b>5</b>	<b>State Feedback NMPC applied to a Diesel Engine</b>	<b>22</b>
5.1	Test Scenario . . . . .	22
5.2	NMPC Design . . . . .	23
5.2.1	NMPC Design without Slew Rate Constraints . . . . .	24
5.2.2	NMPC Design with Slew Rate Constraints . . . . .	25
5.3	Simulation Results . . . . .	29

<i>Contents</i>	vi
5.3.1 Simulation Results without Slew Rate Constraints . . . . .	29
5.3.2 Simulation Results with Slew Rate Constraints . . . . .	33
<b>6 Output Feedback NMPC applied to a Diesel Engine</b>	<b>38</b>
6.1 EKF Setup . . . . .	38
6.2 EKF Design . . . . .	39
6.3 Simulation Results . . . . .	40
<b>7 Conclusions</b>	<b>47</b>

# Chapter 1

## Introduction

The main objective in control of diesel engines is to provide the required engine torque with minimal fuel consumption under the constraint of meeting the given exhaust gas and noise emission laws [22]. While the latter requirement becomes stronger, an emissions aftertreatment is necessary.

Many strategies have been proposed, see e.g. [21] for a survey, how to deal with this problem. One solution is to introduce an exhaust gas recirculation (EGR) which allows to reduce the formation of emissions and a variable geometry turbocharger (VGT) which is used to provide the demanded engine torque. As this solution results in emissions decrease, it creates a strongly coupled nonlinear system. Higher performance benefit can be achieved when the coupled nature between EGR and VGT can be considered in the controller synthesis, as reported by [36]. One would therefore attempt to consider this coupling in the control loop.

The main problems involved in designing a suitable control strategy are the nonlinear multivariable nature of the problem and the presence of constraints on inputs and process variables [17, 21]. Various methods have been applied to the control diesel engines. Examples are gain scheduled parameter-varying control [21, 20], robust  $\mathcal{H}_\infty$  control [36], linear model predictive control [32], backstepping based control [16], nonlinear control Lyapunov function based control [18, 19], adaptive control approaches [3], and nonlinear passivity based control [24, 23]. All these approaches share one common property, namely they can not

directly consider constraints. A possibility to consider constraints in the control problem is to choose nonlinear model predictive control (NMPC). NMPC is especially suited for the control of nonlinear systems subject to input and state constraints [1, 2, 27, 29, 30, 12]. The basic idea of NMPC is to solve at each time instant a finite horizon optimal control problem for the current state. The first part of the resulting open loop optimal control input is applied to the system until the next sampling instant, at which the finite horizon optimal control problem is solved again for the new state. Traditional application areas for NMPC are limited to control problems with rather slow dynamics, e.g. in process control [12]. This is due to the computational load which is assigned with solving the nonlinear and nonconvex optimization problem at each sampling instant.

Therefore, the purpose of this work is twofold. First to study the achievable performance by applying NMPC for a diesel engine control. This may be considered as a benchmark for other control methods. Second, to consider diesel engine control also as the benchmark problem for NMPC itself, motivated by the long term goal to apply NMPC to control problems with fast dynamics. As it has been shown on gasoline engine in [25], NMPC strategy applied on the diesel engine may bring expected benefit.

The remainder of the diploma thesis is structured as follows: In Chapter 2 the overall control problem of a diesel engine is introduced. A model of a diesel engine with exhaust gas recirculation and variable geometry turbocharger is described in Chapter 3. In Chapter 4 the basic idea of NMPC is given. Firstly, in Chapter 5 NMPC is applied to control a diesel engine with state feedback and secondly, in Chapter 6 with output feedback. Finally, conclusions and outlook are given in Chapter 7.

## Chapter 2

# Control Problem

The structure of a diesel engine is shortly presented in this chapter. In particular, the functions of an exhaust gas recirculation and a variable geometry turbocharger are explained and consequently the control problem is formulated.

### 2.1 Principle of EGR and VGT in Diesel Engine

A simplified drawing of the diesel engine is depicted in Figure 2.1. For more details about the structure of the engine and for further explanations the reader is referenced to [33, 17, 22, 21, 19]. As it can be seen from Figure 2.1 modern diesel engines are equipped with an exhaust gas recirculation (EGR) valve and a variable geometry turbocharger (VGT). The EGR valve connects the exhaust manifold with the intake manifold. By this way the exhaust gas mass flow can be partially recirculated and the resulting mixture of the flows decreases the combustion temperature and consequently the formation of  $\text{NO}_x$ . Hence the required environmental benefit is achieved.

The variable geometry turbocharger (VGT) consists of a compressor and a turbine attached at the same shaft. Higher compressed air is supplied into the cylinders where this larger mass of air can be burnt with larger amount of fuel and produces therefore a larger torque. The turbine with variable geometry vanes uses the energy of exhaust gases to drive the compressor. Through VGT the transferred power can be controlled.

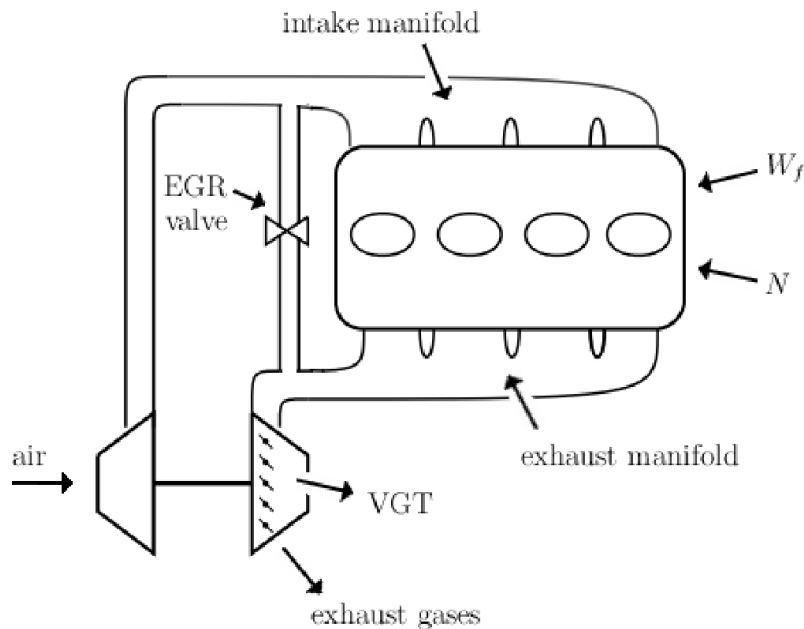


Figure 2.1: A simplified drawing of the turbocharged diesel engine.

## 2.2 Control Problem Formulation

The objective is to maintain the desired torque while the generation of emissions is minimized. This can be done with cooperating the EGR valve and VGT such that performance variables, i.e. burned gas fraction  $F_1$  and air-fuel ratio  $AFR$ , reach their prespecified setpoints. The reduction of harmful nitrogenoxids is achieved with high dilution of the air charge that corresponds to large values of  $F_1$  in the intake manifold [33] while lean AFR lowers the smoke generation through transients.

As described in [33], setpoints for these performance variables are determined via static optimization and their results are stored in static engine maps. Important is, that the setpoints for the performance variables  $F_1$  and  $AFR$  can be precalculated into setpoints for the system state and these values should be tracked with the controller.

According to [22] there are three control loops to be considered: (i) fuel path, (ii) air path and (iii) the EGR path. The air path can be controlled using the turbocharger while the EGR path falls into EGR valve governor. The fuel path is not considered in this simulation study because it is assumed as a known external signal. A scheme of these control loops is

shown in Figure 2.2.

The motivation to use NMPC to control the airpath of a diesel engine comes from its ability to consider constraints in the control problem. The physical restrictions posed for this control problem are actuator limitations, which can vary only between fully open and fully closed, and operational limits due to safety reasons. Classic control approaches aid the manipulated signals with saturation blocks and parameters for the controller are selected after time consuming tuning. Moreover, operational limits cannot be included in these classic control techniques. Another advantage to apply NMPC is that the EGR/VGT coupling is supplied via diesel engine model and thus it may improve the control performance.

Therefore the purpose of this work is to explore the achievable performance of NMPC and to classify it as a benchmark for other control methods. For the comparison two controller design techniques, namely the LQR design and the IO linearization based controller, are used.

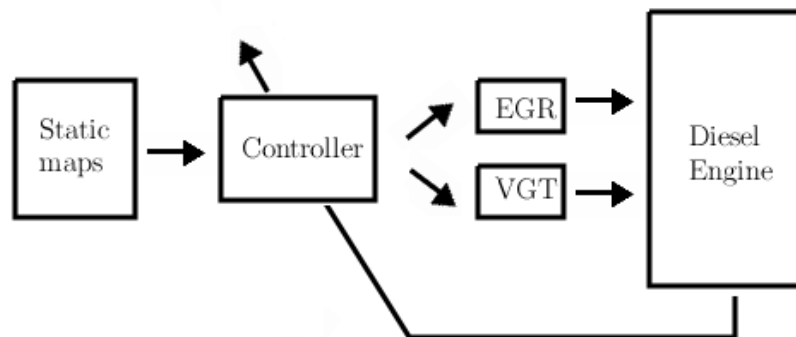


Figure 2.2: Two main control loops, the airpath (controlled via VGT) and the EGR path.

## 2.3 Signal Overview

From the control point of view it is easier to formulate a problem, when the engine is considered as a system with signal definition. Hence, it is necessary to introduce some variables. In the considered diesel engine are located two actuators: the EGR valve and the VGT. The flow of the exhaust gases into the intake manifold can be controlled through the EGR valve. The valve acts between two borders – fully open and fully closed and the position is denoted by a variable  $x_{egr}$ , which ranges from 0 (completely open) to 100% (completely closed). Similarly, actuator situated in the VGT has the same range of validity. It corresponds to the position of a variable noted as  $x_{vgt}$  which varies between 0 and 100%.

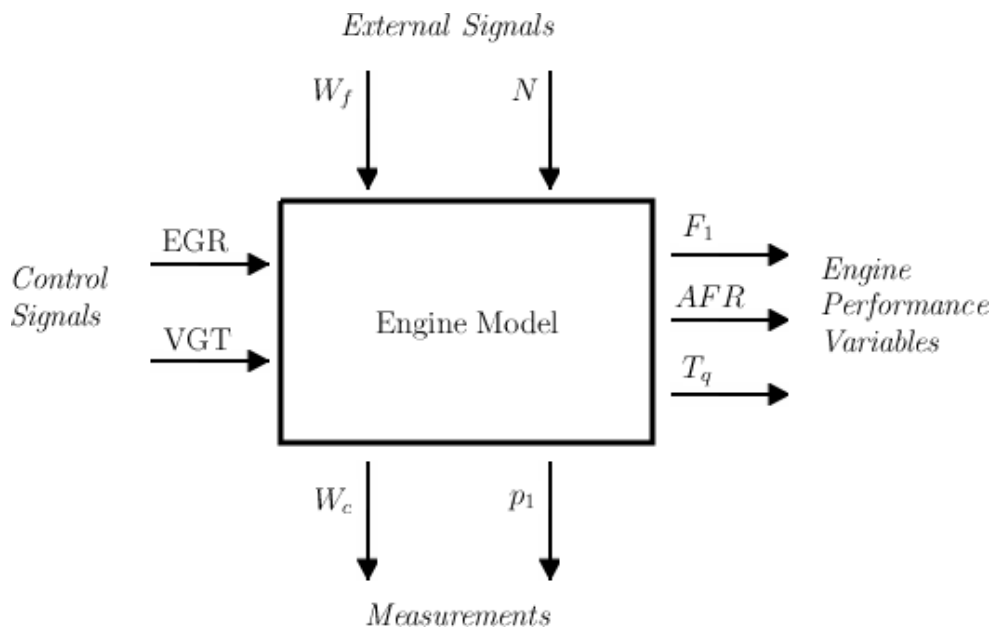


Figure 2.3: Signal routing in the diesel engine.

External inputs represents the engine speed  $N$  and the fuelling rate  $W_f$ . As these inputs can be measured they are treated as measurable disturbances. Furthermore, the measured outputs of the diesel engines are the pressure in the intake manifold  $p_1$  and the mass flow through the compressor  $W_c$ . Variables which specify the engine performance are the burned gas fraction  $F_1$ , the air-fuel ratio  $AFR$  and the engine torque  $T_q$ . The burned gas fraction

is the ratio between the density of the burned gas to the total density of burned gas and air in the intake manifold. It can be written as the following flow fraction

$$F_1 = \frac{W_{egr}}{W_{egr} + W_c}. \quad (2.1)$$

Consequently, the air-fuel ratio equals

$$AFR = (1 - F_1) \frac{k_e p_1}{W_f}. \quad (2.2)$$

The signals are depicted at Fig. 2.3 and relations between them will be explained in the next chapter. After short overview of the control problem, the emphasise in the next chapter will be given specifically to a simplified diesel engine model. This model will be then used for NMPC design in the sequel.

## Chapter 3

# Model of a Diesel Engine

In this chapter a simplified version of a diesel engine model is introduced. The model was proposed by [18] and it is derived from ideal gas law, conservation laws of mass and energy, and some experimental maps. Furthermore, the model is transformed to a normalized form which is used in the controller design in the subsequent chapters.

### 3.1 Physical Model

Applying the mass and energy balances between intake and exhaust manifolds, turbocharger dynamics, actuator and sensor dynamics, it is possible to derive two models of the diesel engine. The first one is of the seventh-order, exploited for instance in [4, 33]. The second one, proposed in [18], is of the third-order. The third order model can be derived from the seventh-order model by approximating the turbocharger dynamics as a first order lag. As shown in [21], this simplified model can capture the dynamics of the system at least in the low and medium speed-load region. Thus, to make the controller design easier, the third-order model is adopted and working regions will be selected according to its validity. The model comprises of three state variables, i.e. the intake manifold pressure  $p_1$ , the exhaust manifold pressure  $p_2$  and the compressor power  $P_c$ . Equations are obtained by differentiating the ideal gas law, while the turbocharger dynamics have been approximated by the power transfer with time constant  $\tau$ . Before introducing the equations, some vari-

ables are defined:  $V_1, V_2$  denote the volumes of the intake and exhaust manifolds,  $T_1, T_2$  the temperatures in the intake and exhaust manifolds,  $T_a, p_a$  the ambient temperature and the ambient pressure,  $V_d$  the total displacement volume,  $P_t$  the turbine power,  $W_{vgt}$  the turbine mass flow rate,  $W_{egr}$  the EGR mass flow rate,  $\eta_c, \eta_t$  the compressor and the turbine isentropic efficiencies,  $\eta_m$  the turbocharger mechanical efficiency,  $\eta_v$  the volumetric efficiency,  $c_p, c_v$  the specific heats at constant pressure and volume, and  $R$  the specific gas constant. Hence, the model of the diesel engine is given by

$$\frac{dp_1}{dt} = \frac{RT_1}{V_1} (W_c + W_{egr} - k_e p_1) \quad (3.1)$$

$$\frac{dp_2}{dt} = \frac{RT_2}{V_2} (k_e p_1 - W_{egr} - W_{vgt} + W_f) \quad (3.2)$$

$$\frac{dP_c}{dt} = \frac{1}{\tau} (-P_c + \eta_m P_t) \quad (3.3)$$

with some nonzero initial conditions where the coefficient  $k_e$  is the engine pumping rate which can be approximated by

$$k_e = \frac{\eta_v V_D N}{120 T_1 R}. \quad (3.4)$$

The mass flow  $W_c$  through the compressor depends on the compressor power and pressures and is given by

$$W_c = \frac{\eta_c}{c_p T_a} \frac{P_c}{\left(\frac{p_1}{p_a}\right)^\mu - 1} \quad (3.5)$$

where  $\mu = \frac{c_p - c_v}{c_p}$ . To model the mass flow through the EGR valve standard orifice equations are used, as described in [21]:

$$W_{egr} = \begin{cases} A_{egr}(x_{egr}) \frac{p_2}{\sqrt{RT_2}} \sqrt{2 \frac{p_1}{p_2} \left(1 - \frac{p_1}{p_2}\right)} & \text{if } p_2 \geq p_1 \\ -A_{egr}(x_{egr}) \frac{p_2}{\sqrt{RT_2}} \sqrt{2 \frac{p_2}{p_1} \left(1 - \frac{p_2}{p_1}\right)} & \text{if } p_1 < p_2. \end{cases} \quad (3.6)$$

A this point is important to note that if  $p_1 < p_2$  the mass flow is reverted. This change is indicated by sign change and by inverting the pressure ratio. In equation (3.6)  $A_{egr}$  denotes the effective area of the EGR valve which is a quadratic function of the normalized position  $x_{egr} \in [0, 100]\%$ , i.e.

$$A_{egr} = -1.5 \cdot 10^{-8} x_{egr}^2 + 3.3 \cdot 10^{-6} x_{egr}. \quad (3.7)$$

In order to avoid that the function (3.7) enters equations (3.1), (3.2) directly, the variable  $A_{egr}$  is considered as a manipulated input<sup>1</sup>. According to [21] the turbine flow  $W_{vgt}$  is given by

$$W_{vgt} = (ax_{vgt} + b) \frac{p_2}{p_{ref}} \sqrt{\frac{T_{ref}}{T_2}} \sqrt{2 \frac{p_a}{p_2} \left(1 - \frac{p_a}{p_2}\right)} \left[ c \left( \frac{p_2}{p_a} - 1 \right) + d \right], \quad (3.8)$$

where  $x_{vgt}$  is the position of VGT actuator,  $p_{ref}$  the reference pressure,  $T_{ref}$  the reference temperature and  $a = -13.62 \cdot 10^{-4} \text{ m}^2$ ,  $b = 0.176 \text{ m}^2$ ,  $c = 0.4 \text{ Pa s m}^{-1}$ ,  $d = 0.6 \text{ Pa s m}^{-1}$  are constant parameters. To simplify, the first part of equation (3.8) is replaced by a new variable noted “effective area of the VGT”, and it is defined by

$$A_{vgt} = ax_{vgt} + b. \quad (3.9)$$

As in the EGR case, this variable plays the role of a new manipulated input. Assuming constant turbine efficiency the turbine power is related to its mass flow via the equation

$$P_t = W_{vgt} c_p T_2 \eta_t \left[ 1 - \left( \frac{p_a}{p_2} \right)^\mu \right]. \quad (3.10)$$

The parameters for the given mathematical model are summarized in Tab. 3.1. In the model one more situation may occur. As the pressures  $p_1$  or  $p_2$  will be narrowing the ambient pressure  $p_1 \rightarrow p_a$  or  $p_2 \rightarrow p_a$  the flows in state equations (3.1), (3.2), (3.3) may become infinite and this is not possible in reality. Therefore, to overcome this obstacle, the pressures are restricted to move in the intervals

$$p_1 \in [102, 155] \text{ kPa} \quad (3.11)$$

$$p_2 \in [102, 175] \text{ kPa}, \quad (3.12)$$

where the upper borders were chosen such that the engine will be protected from overboost<sup>2</sup>. Moreover, as shown in [18], it can be shown that the set  $\Omega := \{(p_1, p_2, P_c) : p_1 > p_a, p_2 > p_a, P_c > 0\}$  is invariant, that is, every trajectory starting in  $\Omega$  stays in  $\Omega$  for all  $t$ . The

---

<sup>1</sup>Due to the monotony property of this function, it can be inverted and precalculated directly onto  $x_{egr}$  signal.

<sup>2</sup>The upper borders were chosen without prior knowledge of the engine, but keeping in mind, that there exist some upper bound – this is usually specified by the producer.

parameter	value	dimension
$\eta_c$	0.61	-
$\eta_t$	0.76	-
$\eta_v$	0.87	-
$\eta_m$	0.98	-
$\tau$	0.11	s
$T_1$	313	K
$T_2$	509	K
$c_p$	1.0144	$\text{kJ kg}^{-1} \text{K}^{-1}$
$c_v$	0.7274	$\text{kJ kg}^{-1} \text{K}^{-1}$
$V_d$	0.002	$\text{m}^3$
$V_1$	0.006	$\text{m}^3$
$V_2$	0.001	$\text{m}^3$
$R$	0.287	$\text{kJ kg}^{-1} \text{K}^{-1}$
$T_a$	298	K
$T_{ref}$	298	K
$p_a$	101.3	kPa
$p_{ref}$	101.3	kPa

Table 3.1: Parameter values.

bounds imposed on the manipulated inputs are precalculated from the limits of EGR and VGT valve position and are given by

$$A_{egr} \in [0, 1.8 \cdot 10^{-4}] \text{ m}^2 \quad (3.13)$$

$$A_{vgt} \in [0.04, 0.176] \text{ m}^2. \quad (3.14)$$

From the practical point of view actuators are always limited with slew rate constraints. These restrictions pose the constraints

$$|\dot{x}_{egr}| \leq [0, 100]\%/s \quad (3.15)$$

$$|\dot{x}_{vgt}| \leq [0, 100]\%/s \quad (3.16)$$

to the control problem and are introduced with a purpose to approach the simulation results closer to practice<sup>3</sup>. The listed constraints on the states (3.11), (3.12) and inputs (3.13), (3.14) and slew rate limits (3.15), (3.16) will serve for NMPC formulation problem in the next chapter.

## 3.2 Control Model

From the numerical and control point of view, it is suitable, when the variables vary in some prespecified regions. This property is achieved via change of coordinates, when the desired steady state is shifted to the origin. In other words, new variables are defined by

$$x_1 = \frac{p_1 - p_1^s}{p_1^s} \quad (3.17)$$

$$x_2 = \frac{p_2 - p_2^s}{p_2^s} \quad (3.18)$$

$$x_3 = \frac{P_c - P_c^s}{P_c^s} \quad (3.19)$$

$$u_1 = \frac{A_{egr} - A_{egr}^s}{A_{egr}^s} \quad (3.20)$$

$$u_2 = \frac{A_{vgt} - A_{vgt}^s}{A_{vgt}^s} \quad (3.21)$$

---

<sup>3</sup>The slew rate limits were chosen deliberately slow such that they need to be respected in the control.

and the model (3.1), (3.2), (3.3) is rewritten into

$$\begin{aligned} \dot{x}_1 = & \frac{RT_1}{p_1^s V_1} \frac{\eta_c}{c_p T_a} \frac{P_c^s (1 + x_3)}{\left(\frac{p_1^s}{p_a}\right)^\mu (1 + x_1)^\mu - 1} \\ & + \frac{T_1}{p_1^s V_1} \sqrt{\frac{R}{T_2}} \Psi(x_1, x_2) A_{egr}^s (1 + u_1) - \frac{\eta_v}{120} \frac{V_d}{V_1} N (1 + x_1) \end{aligned} \quad (3.22)$$

$$\begin{aligned} \dot{x}_2 = & \frac{\eta_v}{120} \frac{T_2}{T_1} \frac{V_d p_1^s}{V_2 p_2^s} N (1 + x_1) - \frac{\sqrt{RT_2}}{p_2^s V_2} \Psi(x_1, x_2) A_{egr}^s (1 + u_1) \\ & - \frac{R}{p_2^s p_{ref} V_2} \sqrt{2T_{ref} T_2} \sqrt{p_a p_2^s (1 + x_2) - p_a^2} \\ & \times \left( c \frac{p_2^s}{p_a} (1 + x_2) - c + d \right) A_{vgt}^s (1 + u_2) + \frac{RT_2}{p_2^s V_2} W_f \end{aligned} \quad (3.23)$$

$$\begin{aligned} \dot{x}_3 = & -\frac{1 + x_3}{\tau} + \frac{\eta_m \eta_t c_p}{\tau P_c^s p_{ref}} \left[ 1 - \left( \frac{p_a}{p_2^s (1 + x_2)} \right)^\mu \right] \sqrt{2T_{ref} T_2} \\ & \times \sqrt{p_a p_2^s (1 + x_2) - p_a^2} \left( c \frac{p_2^s}{p_a} (1 + x_2) - c + d \right) A_{vgt}^s (1 + u_2) \end{aligned} \quad (3.24)$$

with zero initial conditions where the function  $\Psi(x_1, x_2)$  is given by

$$\Psi(x_1, x_2) = \begin{cases} \sqrt{2p_1^s p_2^s (1 + x_1)(1 + x_2) - 2(p_1^s)^2 (1 + x_1)^2} & \text{if } x_2 \geq \frac{p_1^s - p_2^s + p_1^s x_1}{p_2^s} \\ -\sqrt{2p_1^s p_2^s (1 + x_1)(1 + x_2) - 2(p_2^s)^2 (1 + x_2)^2} & \text{otherwise.} \end{cases} \quad (3.25)$$

Note that the function (3.25) contains two parts for two different regions and in the closed loop simulation switching between these two terms may cause slight peaks in the transient.

To overcome this problem a sigmoidal function is deployed

$$f_1(\sigma) = \frac{k_1}{1 + e^{-k_2 \sigma}} - \frac{k_1}{2} \quad (3.26)$$

with two parameters  $k_1 = 17.7578$  kPa and  $k_2 = 0.0435$  kPa<sup>-2</sup> which will cover the critical transient. The function argument is given by

$$\sigma = 2p_1^s p_2^s (1 + x_1)(1 + x_2) - 2(p_1^s)^2 (1 + x_1)^2. \quad (3.27)$$

The transient is depicted at the Fig. 3.1 where the borders for the smooth sector were chosen to be as  $\sigma = \pm 50$  kPa<sup>2</sup>. Such approximation of the EGR mass flow does not conspicuously affect the simulation results because the engine stays the major time outside

this critical region. The main reason for the approximation is to avoid possible numerical problems.

Introduced control model is important to design NMPC. To simplify the notations in the next content, the model will be used in a condensed form. But before applying NMPC scheme to a diesel engine, some theoretic background is given in the next chapter.

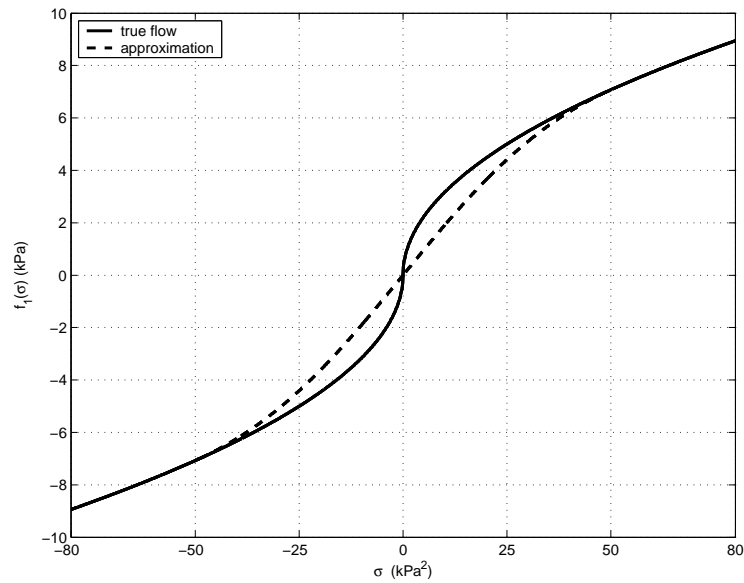


Figure 3.1: Approximation the EGR mass flow with sigmoidal function.

## Chapter 4

# Nonlinear Model Predictive Control

This chapter presents the NMPC basics and a particular interest is focused on the quasi-infinite horizon NMPC scheme. The scheme is explained from two theoretical views in more details. Implementation issues are discussed at the end of the chapter.

### 4.1 NMPC Setup

Consider the time-invariant nonlinear continuous system

$$\dot{\mathbf{x}}(t) = \mathbf{f}(\mathbf{x}(t), \mathbf{u}(t)) \quad (4.1)$$

where the state vector is  $\mathbf{x} \in \mathbb{R}^n$ , the input vector is  $\mathbf{u} \in \mathbb{R}^m$ , satisfying the condition  $\mathbf{f}(\mathbf{0}, \mathbf{0}) = \mathbf{0}$ . The input and state vectors are subjected to the constraints

$$\mathbf{x} \in \mathcal{X}, \quad \mathcal{X} := \{\mathbf{x}_{min} \leq \mathbf{x} \leq \mathbf{x}_{max}\} \quad (4.2)$$

$$\mathbf{u} \in \mathcal{U}, \quad \mathcal{U} := \{\mathbf{u}_{min} \leq \mathbf{u} \leq \mathbf{u}_{max}\}. \quad (4.3)$$

NMPC solves on-line a finite horizon open loop control problem based upon the predictions of the system dynamics (4.1) whereas the constraints (4.2), (4.3) are taken into account as boundary conditions. This problem is solved within each sampling interval and only the first part from the optimized control trajectory is directly applied into the process. Then, based upon the new measurements, the optimization problem is updated and precalculated with new initial conditions.

Practically, there is always a difference between the predicted model-based trajectories and real behaviour of the plant. Thus, to clearly distinguish between these aspects, in the following the predicted trajectories will be denoted with a bar. Starting from these notations, the resulting open-loop optimization problem can be formulated as follows:

$$\min_{\bar{\mathbf{u}}(\cdot)} J = \int_t^{t+T_p} F(\bar{\mathbf{x}}(\tau), \bar{\mathbf{u}}(\tau)) d\tau + G(\bar{\mathbf{x}}(t+T_p)) \quad (4.4)$$

$$\begin{aligned} \text{subject to: } \quad & \dot{\bar{\mathbf{x}}} = \mathbf{f}(\bar{\mathbf{x}}(\tau), \bar{\mathbf{u}}(\tau)), \quad \bar{\mathbf{x}}(t) = \mathbf{x}(t) \\ & \bar{\mathbf{u}}(\tau) \in \mathcal{U}, \quad \forall \tau \in [t, t+T_c] \\ & \bar{\mathbf{u}}(\tau) = \bar{\mathbf{u}}(\tau+T_c), \quad \forall \tau \in [t+T_c, t+T_p] \\ & \bar{\mathbf{x}}(\tau) \in \mathcal{X}, \quad \forall \tau \in [t, t+T_p] \\ & \bar{\mathbf{x}}(t+T_p) \in \mathcal{E} \end{aligned}$$

for a piecewise constant control signal  $\bar{\mathbf{u}}(\cdot)$  with control horizon  $T_c$  and prediction horizon  $T_p$ . The functions  $F$ ,  $G$  can be specified owing to control performance or arising from other considerations.

Stated NMPC formulation does not automatically explain the questions of nominal stability of the closed-loop, robustness and the output feedback. These issues have been resolved by a popular NMPC strategy which guarantees stability and does not require too much computational load and it is called the quasi-infinite horizon NMPC. Related theory background will be briefly reviewed in the next section.

## 4.2 Quasi-Infinite Horizon NMPC Scheme

The underlying idea of quasi-infinite horizon NMPC scheme is to approximate the infinite horizon optimal control with a finite one. It is done with two ingredients: a terminal penalty term  $G(\bar{\mathbf{x}}(t+T_p))$  and a terminal region  $\mathcal{E} = \{\bar{\mathbf{x}} \in \mathcal{R}^n : \bar{\mathbf{x}}^T \mathbf{P} \bar{\mathbf{x}} \leq \alpha\}$ . In other words, the terminal penalty gives an upper bound for the infinite control problem (therefore quasi-infinite horizon) and the terminal region  $\mathcal{E}$  forces the predicted state to reach that region at the end of the prediction horizon.

Mathematically said, for given positive-definite weighing matrices  $\mathbf{Q} \in \mathbb{R}^{n \times n}$ ,  $\mathbf{R} \in \mathbb{R}^{m \times m}$  and terminal penalty symmetric matrix  $\mathbf{P} \in \mathbb{R}^{n \times n}$ , the cost function<sup>1</sup> to be minimized is given by

$$J = \int_t^{t+T_p} \left( \|\bar{\mathbf{x}}(\tau)\|_{\mathbf{Q}}^2 + \|\bar{\mathbf{u}}(\tau)\|_{\mathbf{R}}^2 \right) d\tau + \|\bar{\mathbf{x}}(t+T_p)\|_{\mathbf{P}}^2 \quad (4.5)$$

subject to system dynamics (4.1), input/state constraints (4.2), (4.3) and a terminal inequality constraint

$$\bar{\mathbf{x}}(t+T_p)^T \mathbf{P} \bar{\mathbf{x}}(t+T_p) \leq \alpha \quad (4.6)$$

for some  $\alpha \geq 0$ . The combination of  $\mathbf{Q}$ ,  $\mathbf{R}$ ,  $\mathbf{P}$ ,  $\alpha$  is determined off-line following the quasi-infinity pattern, originally described in [7] which ensures stability and feasibility.

This procedure can be summarized into four steps:

**Step 1** Linearize the system (4.1) to get the Jacobian matrices  $\mathbf{A} = \frac{\partial \mathbf{f}}{\partial \mathbf{x}}(\mathbf{0}, \mathbf{0})$ ,  $\mathbf{B} = \frac{\partial \mathbf{f}}{\partial \mathbf{u}}(\mathbf{0}, \mathbf{0})$ , check the controllability and obtain a linear state feedback control law  $\varphi(\mathbf{x}) = \mathbf{K}\mathbf{x}$ .

**Step 2** Choose a constant  $\kappa \in [0, -\lambda_{\max}(\mathbf{A}_k)]$  for  $\mathbf{A}_k = \mathbf{A} + \mathbf{B}\mathbf{K}$  and solve the Lyapunov function

$$(\mathbf{A}_k + \kappa \mathbf{I})^T \mathbf{P} + \mathbf{P}(\mathbf{A}_k + \kappa \mathbf{I}) = -\mathbf{Q} - \mathbf{K}^T \mathbf{R} \mathbf{K} \quad (4.7)$$

which yields a positive definite matrix  $\mathbf{P}$ .

**Step 3** Solve the optimization problem

$$\max_{\mathbf{x}} \alpha_1 = \mathbf{x}^T \mathbf{P} \mathbf{x} \quad (4.8)$$

such that  $\mathbf{K}\mathbf{x} \in \mathcal{U}$ ,  $\mathbf{x} \in \mathcal{X}$  which specifies the region

$$\mathcal{E}_1 = \{\mathbf{x} \in \mathbb{R}^n : \mathbf{x}^T \mathbf{P} \mathbf{x} \leq \alpha_1\}. \quad (4.9)$$

**Step 4** Find the largest possible  $\alpha \in (0, \alpha_1]$ , determining the region

$$\mathcal{E} = \{\mathbf{x} \in \mathbb{R}^n : \mathbf{x}^T \mathbf{P} \mathbf{x} \leq \alpha\}. \quad (4.10)$$

---

<sup>1</sup>The term  $\|\mathbf{w}\|_{\mathbf{S}}^2 = \mathbf{w}^T \mathbf{S} \mathbf{w}$  denotes a quadratic norm of vector  $\mathbf{w}$  for given positive definite matrix  $\mathbf{S}$ .

and reducing from  $\alpha_1$  until the objective function is negative

$$\begin{aligned} \max_{\mathbf{x}} \quad & \{\mathbf{x}^T \mathbf{P} \xi(\mathbf{x}) - \kappa \mathbf{x}^T \mathbf{P} \mathbf{x}\} \\ \text{s.t.} \quad & \mathbf{x}^T \mathbf{P} \mathbf{x} \leq \alpha \end{aligned} \quad (4.11)$$

where  $\xi(\mathbf{x}) = \mathbf{f}(\mathbf{x}, \mathbf{K}\mathbf{x}) - \mathbf{A}_k \mathbf{x}$  is the difference between the nonlinear and linearized model.

The principle of NMPC is shortly presented here. Further discussion about NMPC problem can be found in [13, 15] and a thorough survey from the past developments with future needs is given for example in [28]. For a detailed view regarding state feedback, output feedback, stability, optimality, the reader is referenced to [14, 27], and references therein.

### 4.3 Computation of the Terminal Region

The size of the terminal region depends strongly on the system nonlinearity. As it directly affects the feasibility condition, one would therefore attempt to calculate the largest terminal region. In particular, it is very difficult, if not impossible, to find the largest terminal region for a given nonlinear system [7]. From the computational point of view, the quasi-infinite pattern leads to a semi-infinite optimization problem which is not easy to solve. The main unresolved difficulty at this point is the determination of the region  $\mathcal{E}$  which appears to require that some global test is satisfied which again may not be trivial except for academic examples [28].

Another way, proposed in [9], offers the determination of the terminal region by the use of linear approximation. The basic idea is to approximate the nonlinear system with a linear differential inclusion (LDI) beyond the prediction horizon. The algorithm results in a LMI optimization problem. Gained advantages are in including the input/state constraints into the problem and moreover, the well-defined convex optimization problem yields global solution. However, as the process is aided with LDI, this may cause some conservativeness. As this aspect depends on the nonlinearity degree, in the further context the proposed

approach will be investigated on the diesel engine model to assure that the terminal region was yielded properly. Consider the nonlinear system (4.1) and define  $\mathbf{A}(t) = \frac{\partial \mathbf{f}}{\partial \mathbf{x}}$ ,  $\mathbf{B}(t) = \frac{\partial \mathbf{f}}{\partial \mathbf{u}}$  for all  $t \in [t + T_p, \infty)$ . Consequently for a defined set  $M \subset \mathbb{R}^{n+m}$  the LDI system is given by

$$\Theta(M) := \left\{ \mathbf{F}(t), \begin{bmatrix} \mathbf{x} \\ \mathbf{u} \end{bmatrix} \in M, t \in [t + T_p, \infty) \right\} \quad (4.12)$$

where  $\mathbf{F}(t) = [\mathbf{A}(t) \ \mathbf{B}(t)]$ . State and input constraints are assumed to be symmetric and the constraint set is specified as

$$\Gamma := \{ \mathbf{x} \in \mathbb{R}^n : (\mathbf{h}_i + \mathbf{l}_i \mathbf{K}) \mathbf{x} \leq 1, i = 1, \dots, r \} \quad (4.13)$$

where  $\mathbf{h}_i, \mathbf{l}_i$  denotes the linear box constraints imposed on the states/inputs and  $r$  is the number of constraints. The LMI procedure is then as follows:

**Step 1** Choose the set  $\Gamma$  with symmetric constraints as in (4.13) such that the size of this region will be considered as the feasible region for the LMI problem<sup>2</sup>.

**Step 2** Approximate the process (4.1) with LDI (4.12) which is subjected to the set  $\Gamma$ .

**Step 3** Determine the convex hull  $Co\Theta(\Gamma)$ , given as

$$Co\Theta(\Gamma) := \left\{ \begin{array}{l} \mathbf{F}(t) \in \mathbb{R}^{n \times (n+m)} : \mathbf{F}(t) = \sum_{i=1}^{N_e} \beta_i \mathbf{F}_i = \sum_{i=1}^{N_e} \beta_i [\mathbf{A}_i \ \mathbf{B}_i] \\ \beta_i \geq 0, \sum_{i=1}^{N_e} \beta_i = 1, t \in [t + T_p, \infty) \end{array} \right\} \quad (4.14)$$

where  $\mathbf{F}_i = [\mathbf{A}_i \ \mathbf{B}_i]$  are the extreme matrices of the linear approximation.  $N_e$  is the number of extreme combinations of  $\mathbf{F}$ .

**Step 4** Solve the LMI optimisation problem

$$\begin{array}{ll} \max_{\alpha, \mathbf{W}_{1\alpha}, \mathbf{W}_{2\alpha}} & \log \det(\mathbf{W}_{1\alpha}) \\ \text{s. t.} & \mathbf{W}_{1\alpha} > 0, \alpha > 0 \end{array} \quad (4.15)$$

---

<sup>2</sup>If the set is too large, the LMI problem is infeasible, else if it is too small, also the terminal region is going to be small. Furthermore, this selection indicates the region of validity of LDI approximation.

with conditions

$$\begin{bmatrix} -\mathbf{F}_i \mathbf{W}_\alpha^T - \mathbf{W}_\alpha \mathbf{F}_i^T & \begin{bmatrix} \mathbf{W}_{1\alpha} \mathbf{Q}^{1/2} & \mathbf{W}_{2\alpha}^T \end{bmatrix} \\ \begin{bmatrix} \mathbf{Q}^{1/2} \mathbf{W}_{1\alpha} \\ \mathbf{W}_{2\alpha} \end{bmatrix} & \begin{bmatrix} \alpha \mathbf{I} & \mathbf{0} \\ \mathbf{0} & \alpha \mathbf{R}^{-1} \end{bmatrix} \end{bmatrix} \geq 0, \quad i = 1, \dots, N_e \quad (4.16)$$

$$\begin{bmatrix} 1 & \mathbf{h}_i \mathbf{W}_{1\alpha} + \mathbf{l}_i \mathbf{W}_{2\alpha} \\ (\mathbf{h}_i \mathbf{W}_{1\alpha} + \mathbf{l}_i \mathbf{W}_{2\alpha})^T & \mathbf{W}_{1\alpha} \end{bmatrix} \geq 0, \quad i = 1, \dots, r \quad (4.17)$$

where  $\mathbf{W}_\alpha = [\mathbf{W}_{1\alpha} \ \mathbf{W}_{2\alpha}^T]$ .

**Step 5** Determine the terminal matrix  $\mathbf{P}$  from

$$\mathbf{P} = \alpha \mathbf{W}_{1\alpha}^{-1} \quad (4.18)$$

and the state feedback gain

$$\mathbf{K} = \mathbf{W}_{2\alpha} \mathbf{W}_{1\alpha}^{-1}. \quad (4.19)$$

while  $\alpha$  is yielded directly from the optimization problem.

The LMI approach to quasi-infinite horizon NMPC scheme is presented in this section. For detailed description the reader is referenced to original papers [8, 9].

## 4.4 NMPC Implementation

Further discussions emerge about NMPC optimization strategies, see for instance a survey in [5]. Many of them use direct solution methods using a finite parametrization of control inputs, states and constraints. In this category falls also called simultaneous strategy which discretises the control and state variables using polynomials and transforms the problem into large nonlinear problem (NLP). In this work the DYNOPT optimization package [10] is employed. The underlying principle of this code is the transformation using orthogonal collocation on finite elements method and hence total discretisation. The routine is developed under MATLAB environment and uses fmincon function provided by

Optimization Toolbox to solve a specially tailored dynamic optimization problem. The DYNOPT code solves the following general optimal control problem for  $t \in [t_0, t_f]$ :

$$\min_{\mathbf{u}(t)} \{\mathcal{G}(\mathbf{x}(t_f), t_f)\} \quad (4.20)$$

subject to

$$\begin{aligned} \dot{\mathbf{x}}(t) &= \mathbf{f}(t, \mathbf{x}(t), \mathbf{u}(t)), & \mathbf{x}(t_0) &= \mathbf{x}_0 \\ \mathbf{h}(t, \mathbf{x}(t), \mathbf{u}(t)) &= \mathbf{0} \\ \mathbf{g}(t, \mathbf{x}(t), \mathbf{u}(t)) &\leq \mathbf{0} \\ \mathbf{x}_{lb}(t) &\leq \mathbf{x}(t) \leq \mathbf{x}_{ub}(t) \\ \mathbf{u}_{lb}(t) &\leq \mathbf{u}(t) \leq \mathbf{u}_{ub}(t) \end{aligned}$$

where  $\mathbf{h}$  is an equality constraint,  $\mathbf{g}$  is an inequality constraint,  $\mathbf{x}_{lb}(t), \mathbf{x}_{ub}(t)$  are state constraints, and  $\mathbf{u}_{lb}(t), \mathbf{u}_{ub}(t)$  are control constraints.

Furthermore, in order to speed up the optimizer for NMPC implementation, a non-equidistant partitioning of the prediction horizon is used. The decomposition is based on a geometric sequence such that the length of first subinterval equals the sampling time and the sum of all subintervals equals the prediction length.

## Chapter 5

# State Feedback NMPC applied to a Diesel Engine

This chapter describes the test scenario for the diesel engine and proceeds into details of NMPC design. Assuming that all state are available for control purposes, the diesel engine is controlled firstly without consideration of slew rate constraints and secondly with slew rate constraints. Results are shown respectively in subsequent sections.

### 5.1 Test Scenario

To obtain setpoints, the derivatives in (3.1), (3.2) and (3.3) are set equal to zero and solved using MATLAB function `fsolve`. The test scenario is considered as a sequence of setpoint changes. It is expected that the constraints (3.13), (3.14) become active through transients because the selected setpoints are close to the allowable bounds. The Table 5.1 summarizes the setpoint values.

The objective of the control design is to drive the system (3.1), (3.2), (3.3) between selected setpoints (5.1) such that the input and state constraints will be satisfied. In this scenario is assumed that no noise enters the process and therefore the nominal performance is investigated. Moreover, the computational delays are neglected. Simulations will be divided into a serie where the results presentation has the following sequence:

variable	setpoint 1	setpoint 2	setpoint 3
$x_{egr}$ [%]	12.87	72.14	3.07
$x_{vgt}$ [%]	70	10	86
$A_{egr}$ [m <sup>2</sup> ]	$0.4 \cdot 10^{-4}$	$1.6 \cdot 10^{-4}$	$0.1 \cdot 10^{-4}$
$A_{vgt}$ [m <sup>2</sup> ]	0.0807	0.1624	0.0589
$W_f$ [kg h <sup>-1</sup> ]	4	6	5
$N$ [rpm]	1900	2100	2000
$p_1$ [kPa]	123.17	107.44	146.86
$p_2$ [kPa]	131.37	108.97	171.59
$P_c$ [W]	932.0	239.6	2480.8

Table 5.1: Setpoint values.

1. State feedback without considering slew rate limits
2. State feedback with slew rate constraints
3. Output feedback with slew rate constraints.

The engine behaviour will be tested within three synthetise techniques:

1. LQR design
2. IO linearisation
3. NMPC.

In order to present clear results and to overcome the density of the lines due to the fast dynamics Fig. 5.1 shows the desired trajectories for two measured outputs. These setpoint lines will be omitted in the figures.

## 5.2 NMPC Design

To avoid numerical problems with the terminal region calculation and to obtain satisfactory results, a combination with LMI approach is deployed. The quasi-infinite pattern is used

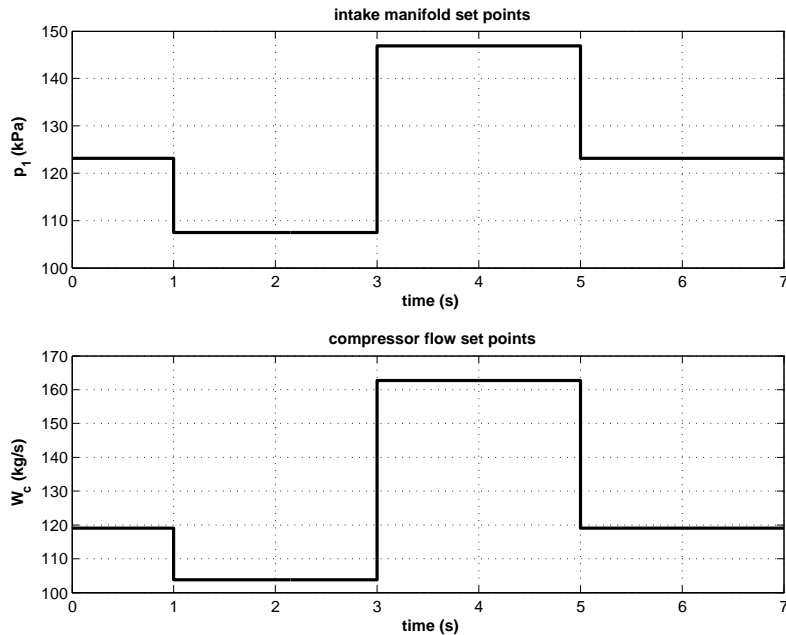


Figure 5.1: Test scenario.

until the step three and from that point the LMI procedure is applied such that  $\alpha = \alpha_1$  is fixed in the optimization problem (4.15). Fixing  $\alpha$  in the LMI optimization problem reduces the conservativeness of the LDI approximation while  $\alpha_1$  ensures the maximum volume of the terminal region (4.9). Results obtained by this way will be depicted at the end of this section to check the validity.

### 5.2.1 NMPC Design without Slew Rate Constraints

The stage cost for NMPC design is chosen to be

$$\mathbf{Q} = \text{diag}(1 \ 1 \ 1), \quad \mathbf{R} = \text{diag}(1 \ 1). \quad (5.1)$$

For the diesel engine model (3.22), (3.23), (3.24) the quasi-infinite horizon NMPC pattern is applied until the third step. This procedure is repeated for each setpoint and the following constants are obtained

$$\alpha_1 = 10.9579, \quad \alpha_2 = 0.2699, \quad \alpha_3 = 0.0913, \quad (5.2)$$

which specify the region  $\mathcal{E}_1$  in (4.9). Afterwards it is proceeded with the LMI approach. Firstly, the constraint set (4.13) is selected. For this purpose a symmetric constraints based upon the nearest border is selected, i.e.

$$\mathbf{x}_b = 0.9 \min (|\mathbf{x}_{min}|, |\mathbf{x}_{max}|) \quad (5.3)$$

$$\mathbf{u}_b = \min (|\mathbf{u}_{min}|, |\mathbf{u}_{max}|) \quad (5.4)$$

where  $\mathbf{x}_b$ ,  $\mathbf{u}_b$  are the imposed bounds on the states and inputs, respectively. Secondly the process (3.22), (3.23), (3.24) is transformed into LDI (4.12). The convex hull is determined with  $N_e = 2^{n+m} - 8$  combinations of extremes matrices where the number 8 denotes omitted cases where  $p_{1max} > p_{2min}$  because this is practically not true. For given weighing matrices (5.1) the LMI problem (4.15) is solved via the YALMIP routine [26] with fixed constants (5.2) and the following matrices are obtained

$$\begin{aligned} \mathbf{P}_1 &= \begin{pmatrix} 485.0356 & 71.9058 & -29.6126 \\ 71.9058 & 282.2638 & -12.8852 \\ -29.6126 & -12.8852 & 78.9288 \end{pmatrix}, \quad \mathbf{P}_2 = \begin{pmatrix} 1191.380 & 293.252 & -24.989 \\ 293.252 & 377.284 & -18.302 \\ -24.989 & -18.302 & 89.282 \end{pmatrix}, \\ \mathbf{P}_3 &= \begin{pmatrix} 36.6920 & -0.0002 & -0.0000 \\ -0.0002 & 284.8366 & -0.0001 \\ -0.0000 & -0.0001 & 2.5724 \end{pmatrix}. \end{aligned} \quad (5.5)$$

The penalty matrices (5.5) will be used for NMPC problem and as depicted in Figures 5.2, 5.3, 5.4 the volume of such achieved ellipsoids exactly fills the space between the state borders (5.3). Thus it may be concluded that the regions are calculated properly. In the online simulation the prediction horizons were chosen

$$T_p = 0.9 \text{ s}, \quad T_c = 0.9 \text{ s}. \quad (5.6)$$

### 5.2.2 NMPC Design with Slew Rate Constraints

To be able to include slew rate constraints in NMPC, the control problem needs to be modified. A common way is to augment the plant with virtual inputs, i.e. to define

$$\mathbf{v} = [\dot{u}_1(t) \ \dot{u}_2(t)]^T \quad (5.7)$$

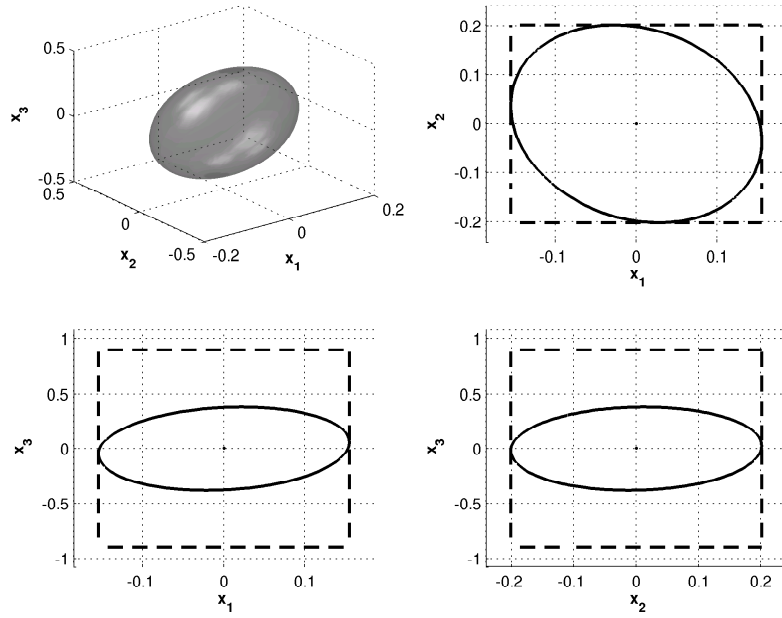


Figure 5.2: Terminal region for the setpoint 1.

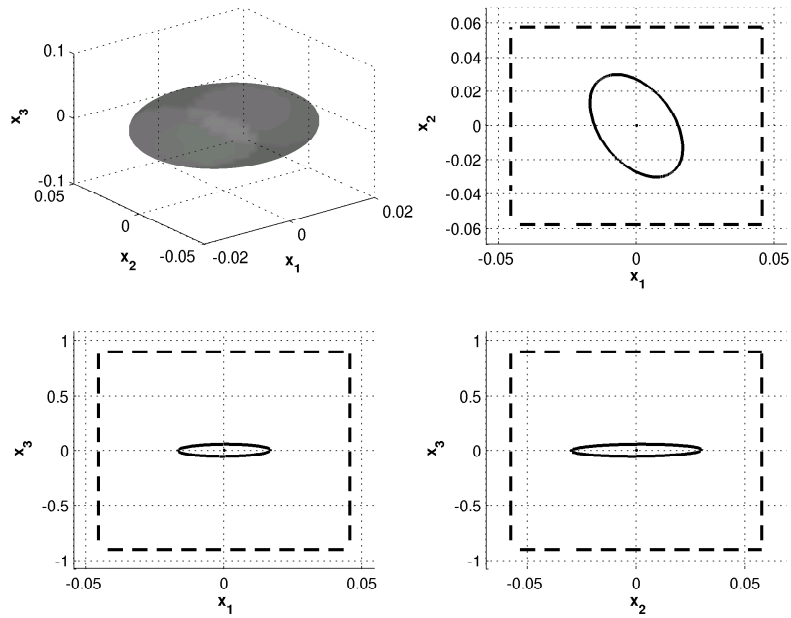


Figure 5.3: Terminal region for the setpoint 2.

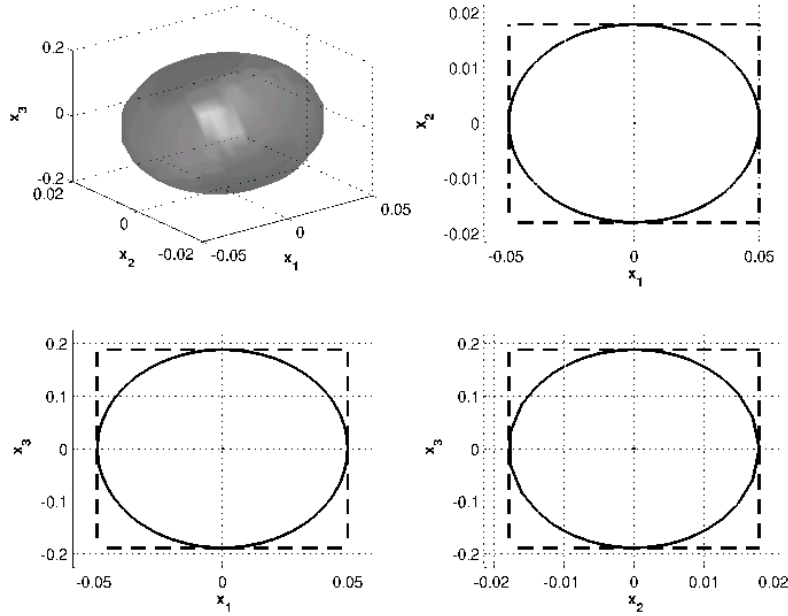


Figure 5.4: Terminal region for the setpoint 3.

and transform the model (3.22), (3.23), (3.24) into a larger one where the previous state vector contains now five state variables

$$\mathbf{z} = [x_1 \ x_2 \ x_3 \ u_1 \ u_2]^T. \quad (5.8)$$

The new augmented system becomes

$$\dot{\mathbf{z}} = \tilde{\mathbf{f}}(\mathbf{z}, \mathbf{v}), \quad \mathbf{z}(\mathbf{0}) = \mathbf{0} \quad (5.9)$$

which satisfies the condition  $\tilde{\mathbf{f}}(\mathbf{0}, \mathbf{0}) = \mathbf{0}$ . In the model (5.9) the slew rate constraints can be viewed as bounds for the virtual inputs whilst the previous input limits (3.13), (3.14) are treated as state constraints.

In the next step, new weights are introduced

$$\mathbf{Q} = \text{diag}(1 \ 1 \ 1 \ 1 \ 1), \quad \mathbf{R} = \text{diag}(0.1 \ 0.1) \quad (5.10)$$

and the quasi-infinite pattern is progressed until the third step. Solving the problem (4.8) which is subjected to the augmented state (5.8) with respective bounds, following constants

are obtained

$$\alpha_1 = 0.0405, \quad \alpha_2 = 0.0092, \quad \alpha_3 = 0.0522. \quad (5.11)$$

The LMI procedure starts with the constraint set selection

$$\mathbf{z}_b = 0.9 \min(|\mathbf{z}_{min}|, |\mathbf{z}_{max}|) \quad (5.12)$$

$$\mathbf{v}_b = \min(|\mathbf{v}_{min}|, |\mathbf{v}_{max}|) \quad (5.13)$$

and the convex hull (4.14) is determined (omitting the cases where  $p_{1max} > p_{2min}$ ). The LMI optimization problem is solved (4.15) with fixed  $\alpha$  and following matrices are obtained

$$\begin{aligned} \mathbf{P}_1 &= \begin{pmatrix} 1.7987 & -0.1172 & 0.1026 & 0.0000 & -0.0553 \\ -0.1172 & 1.0163 & -0.0079 & 0.0000 & 0.0598 \\ 0.1026 & -0.0079 & 0.1132 & 0.0000 & -0.0172 \\ 0.0000 & 0.0000 & 0.0000 & 0.3162 & -0.0000 \\ -0.0553 & 0.0598 & -0.0172 & -0.0000 & 0.3394 \end{pmatrix}, \\ \mathbf{P}_2 &= \begin{pmatrix} 4.4854 & -0.0753 & 0.0748 & -0.0000 & -0.0544 \\ -0.0753 & 2.7840 & 0.0017 & -0.0000 & -0.0011 \\ 0.0748 & 0.0017 & 0.1599 & 0.0000 & -0.0189 \\ -0.0000 & -0.0000 & 0.0000 & 0.7290 & -0.0000 \\ -0.0544 & -0.0011 & -0.0189 & -0.0000 & 1.6284 \end{pmatrix}, \\ \mathbf{P}_3 &= \begin{pmatrix} 20.9696 & 0.0000 & -0.0000 & -0.0000 & 0.0000 \\ 0.0000 & 162.7848 & 0.0000 & 0.0000 & -0.0000 \\ -0.0000 & 0.0000 & 1.4701 & -0.0000 & -0.0000 \\ -0.0000 & 0.0000 & -0.0000 & 0.0644 & 0.0000 \\ 0.0000 & -0.0000 & -0.0000 & 0.0000 & 0.6135 \end{pmatrix}. \end{aligned} \quad (5.14)$$

Prediction horizons with respect to slew rate constraints are prolonged to

$$T_p = 1.5 \text{ s}, \quad T_c = 1.5 \text{ s}. \quad (5.15)$$

Without further discussion the sampling time (with or without slew rate limits considerations) is chosen equal  $T_s = 0.01 \text{ s}$  but for a more detailed view the reader is referenced to [17].

## 5.3 Simulation Results

In this section the performance of NMPC, LQR and IO-based controller are compared. The LQR controller is designed for every setpoint with same weights as for NMPC controller. Derivation of the IO-based controller is performed in [6] and only achieved results are discussed. Adjustment of the IO-based controller is made to be as fast as in the LQR case, e.g. the similar behaviour is pretuned for every controller. Except for NMPC controller the control signals are clipped with saturation blocks. Dashed lines on the graphs will be reserved for the inputs/states bounds.

### 5.3.1 Simulation Results without Slew Rate Constraints

The trajectory of the exhaust manifold pressure in Fig. 5.6 during the second changeover clearly confirms that the LQR controller does not respect the upper limit and the diesel engine suffers overboost. This is not the case in NMPC control and the controller holds the diesel engine in the safety region and benefits from its strong advantage – to handle constraints. Comparing the rest between the LQR and NMPC there is no significant difference. At this point suits the claim from [11]: In many cases the nonlinear receding horizon controller may represent a more sophisticated alternative to an existing LQ regulator designed on the linearized plant. IO linearisation behaves slower comparing to LQR or NMPC and the setpoints are touched with some delay. The same can be seen also on transients in intake manifold pressure (Fig. 5.5) or in Fig. 5.7. This delay appears because only one IO-based controller is designed for every setpoint and no switching is executed as in the LQR case.

In Fig. 5.8 there is a significant inverse response in the LQR/NMPC for the first changeover. An explanation of this peak is a matter of fact that in the control problem no slew rate constraints are considered. IO-based controller does not manifest this behaviour and performs better. However, when comparing the signals into actuators, namely EGR signals in Fig. 5.9 and VGT signals in Fig. 5.10, it can be concluded that none from the controllers suits the practice. Thus, it is necessary to include slew rate limits into the control problem.

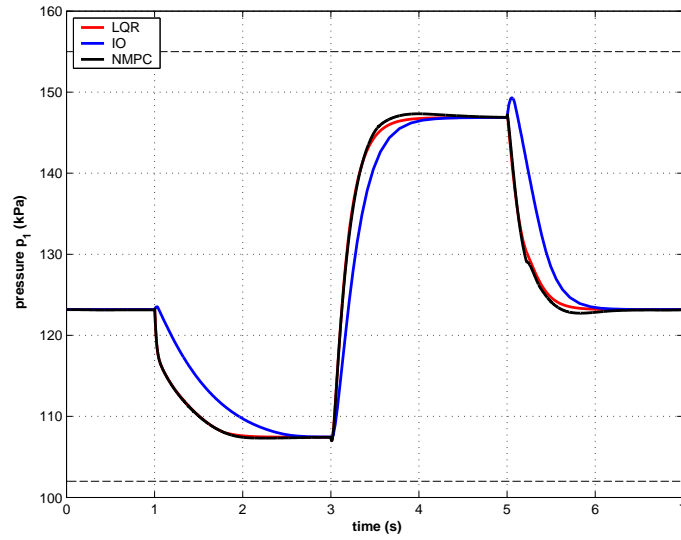


Figure 5.5: Control of the intake manifold pressure (without slew rate constraints).

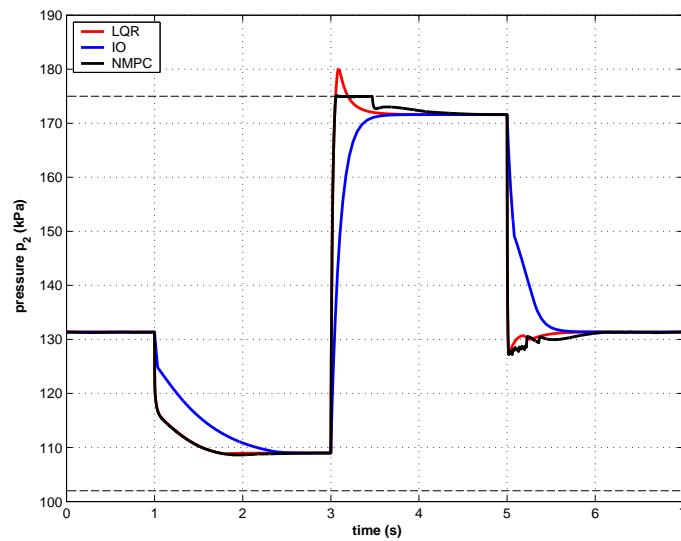


Figure 5.6: Control of the exhaust manifold pressure (without slew rate constraints).

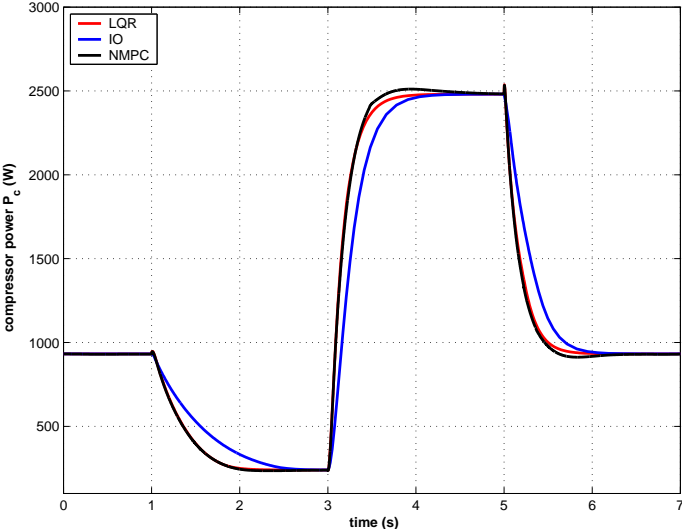


Figure 5.7: Control of the compressor power (without slew rate constraints).

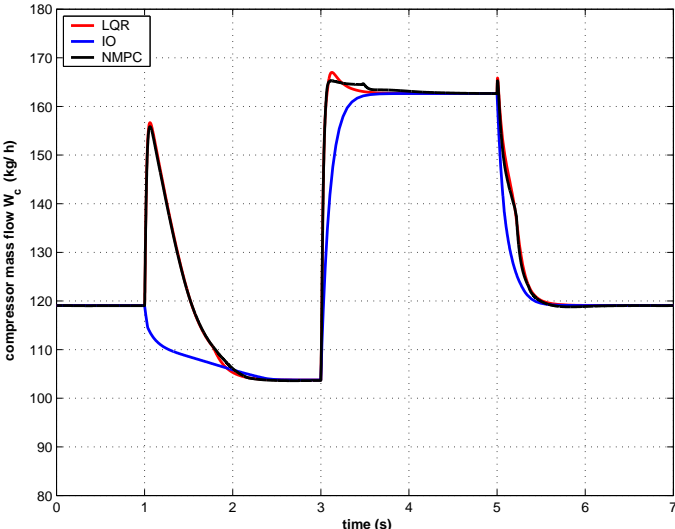


Figure 5.8: Control of the compressor mass flow (without slew rate constraints).

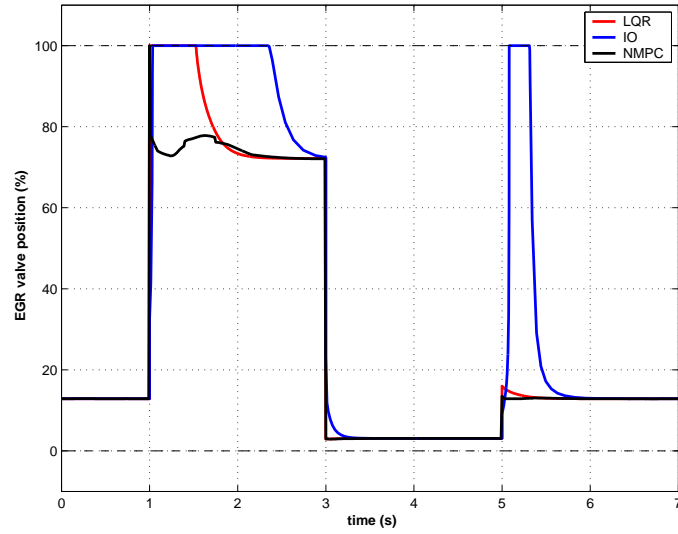


Figure 5.9: Signals for the EGR valve (without slew rate constraints).

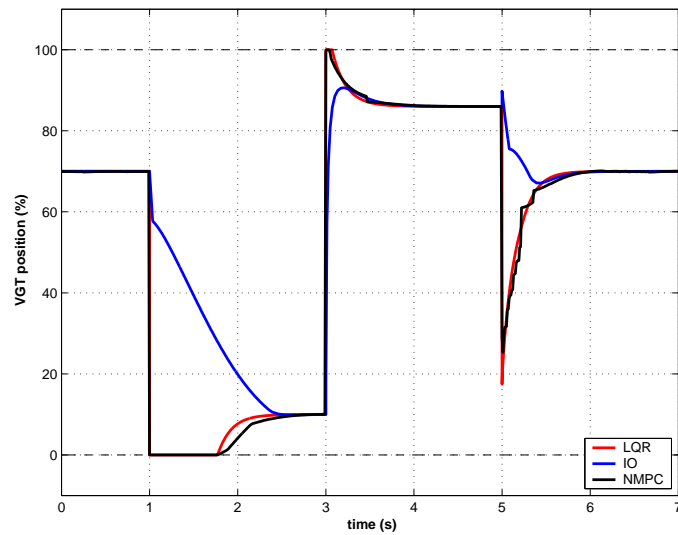


Figure 5.10: Signals for the VGT (without slew rate constraints).

### 5.3.2 Simulation Results with Slew Rate Constraints

In order to consider slew rate constraints into the control problem also the LQR controller is precalculated for augmented plant (5.9). The weights are chosen the same as in NMPC control (5.10) and the controller is designed for every setpoint. The IO-based controller is adjusted such that the performance is similar to LQR/NMPC. A rate limiter is employed to limit the rise/fall in the LQR and IO case.

Figure 5.11 depicts the pressure in the intake manifold during the changeovers. Similarly as in the previous simulation study (without the slew rate constraints), transients of LQR and NMPC are obviously close to each other. The same behaviour can be seen on transients in exhaust manifold pressure in Fig. 5.12. In this figure none from the controllers exceeds the upper bound. This might not happen for LQR or IO controller if they were a bit more aggressively tuned. The transients in compressor power in Fig. 5.13 show that IO-based controller acts is a bit slower.

Including slew rate constraints brings an expected benefit when looking in Fig. 5.14. The inverse response for the first changeover is significantly reduced and approaches the simulation closer to practice. Comparing the signals for EGR valve in Fig. 5.15 and for VGT in Fig. 5.16 there can be seen as the slew rate constraints are active in every setpoint change. More detailed view offers Fig. 5.17 with EGR control moves and Fig. 5.18 with VGT control moves.

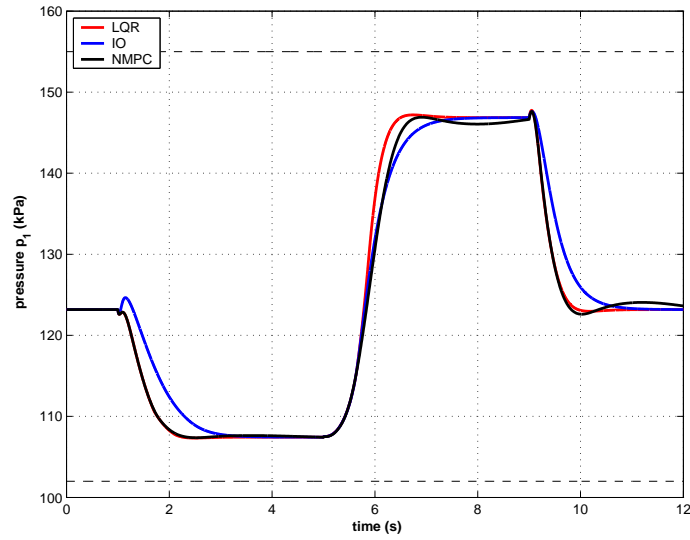


Figure 5.11: Control of the intake manifold pressure (with slew rate constraints).

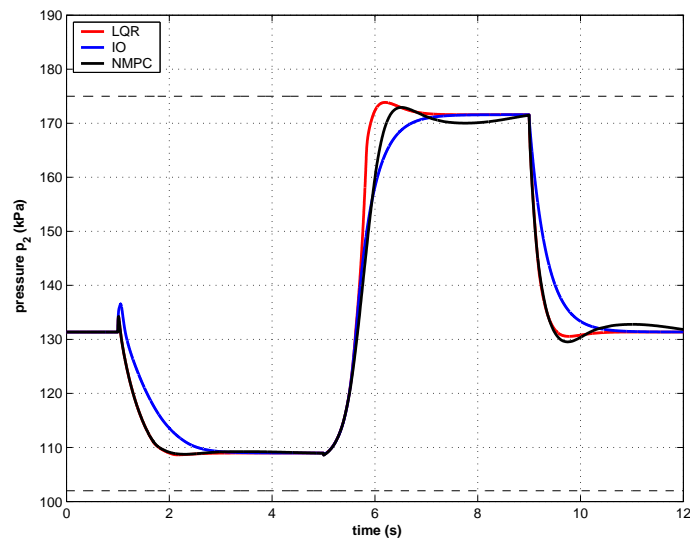


Figure 5.12: Control of the exhaust manifold pressure (with slew rate constraints).

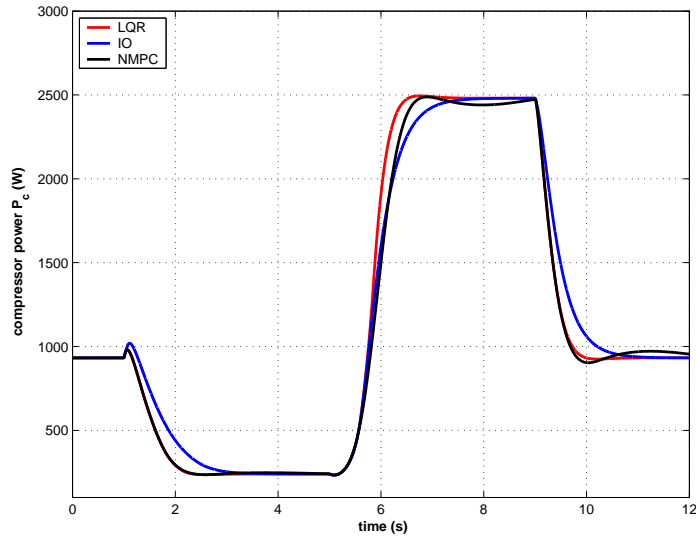


Figure 5.13: Control of the compressor power (with slew rate constraints).

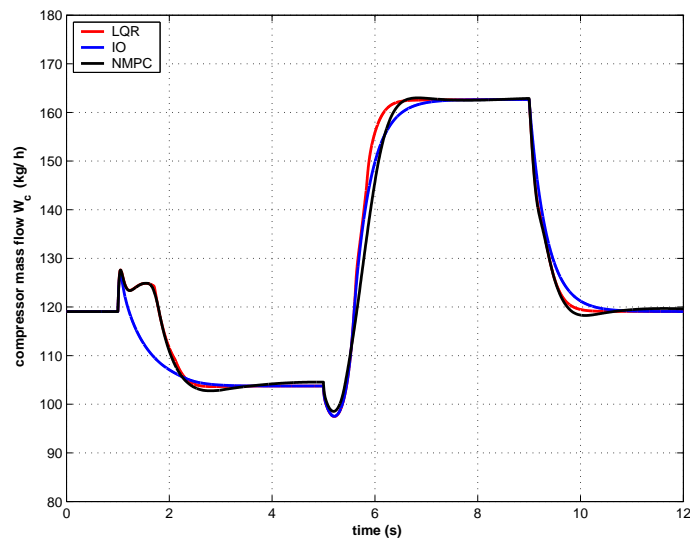


Figure 5.14: Control of the compressor mass flow (with slew rate constraints).

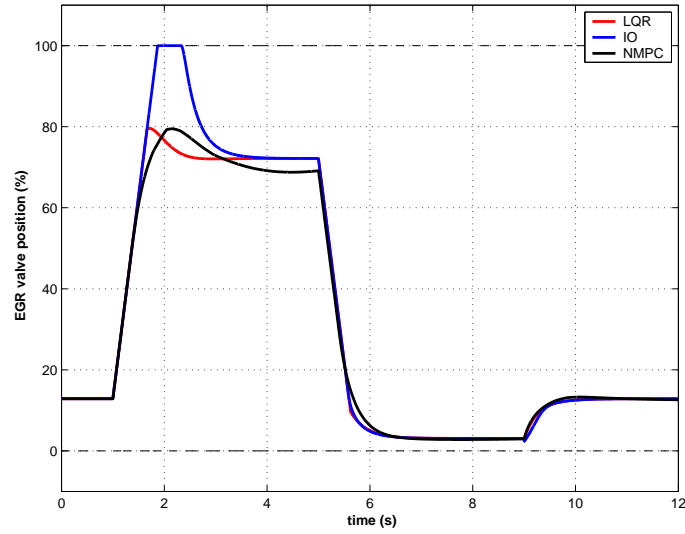


Figure 5.15: Signals for the EGR valve (with slew rate constraints).

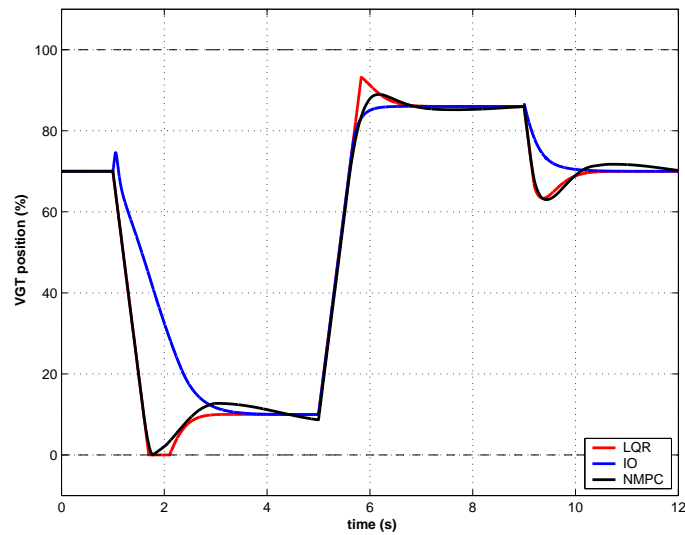


Figure 5.16: Signals for the VGT (with slew rate constraints).

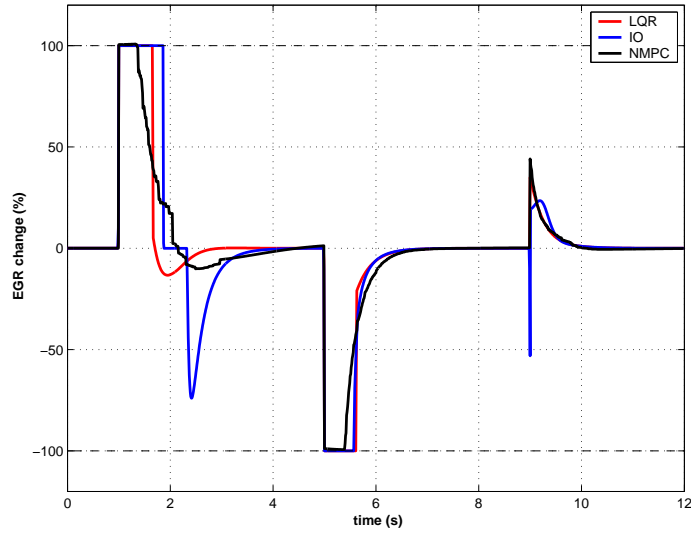


Figure 5.17: EGR control moves (with slew rate constraints).

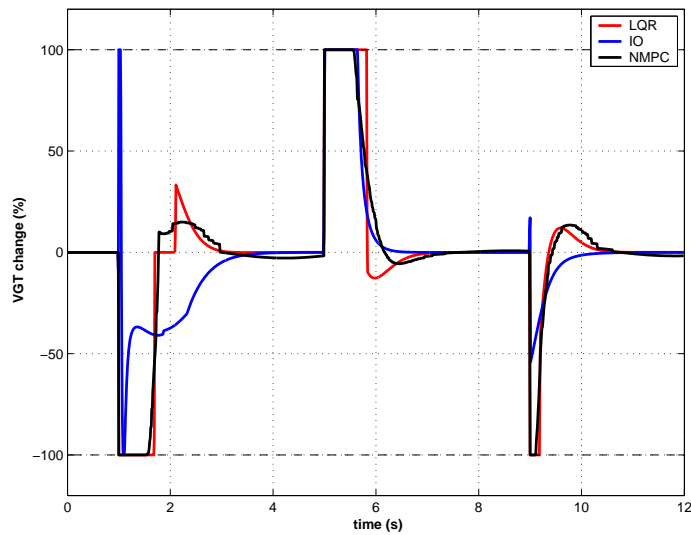


Figure 5.18: VGT control moves (with slew rate constraints).

## Chapter 6

# Output Feedback NMPC applied to a Diesel Engine

An extended Kalman filter (EKF) serves to recover states for output feedback NMPC in this chapter. The observer is tested with additional noise and shows satisfactory results. The controller performance of NMPC control in considering with the EKF is studied and simulation results are provided.

### 6.1 EKF Setup

To apply NMPC all current states have to be supplied. However, not all states are directly measurable and in this case only the measurements of the intake manifold pressure and the massflow through the compressor can be provided. Thus an observer is needed. The estimation task here is more challenging than in gasoline engine due to the interaction of the intake, turbocharger and exhaust manifold dynamics [34]. In this work the diesel engine is considered as a mean value model and it is not proceeded further into the estimation problematics. This topic is for instance thoroughly exploited for a diesel engine without EGR in [34, 35, 17].

An extended Kalman filter with slight modifications is employed, as suggested in [31]. Claiming authors, these modifications have two advantages, namely the degree of stability

can be prescribed in advance and the nonlinearities can be tackled in a more effective way. In the following the principle of the EKF will be briefly presented but for the complete structure of the estimation problem the reader is referenced to the original paper [31]. The estimated states will be noted with a hat. For the considered system (4.1) the EKF is given by

$$\dot{\hat{\mathbf{x}}}(t) = \mathbf{f}(\hat{\mathbf{x}}(t), \mathbf{u}(t)) + \mathbf{L}(t)(\mathbf{y}(t) - \hat{\mathbf{y}}(t)) \quad (6.1)$$

where  $\mathbf{y}(t)$  is a vector of measurements,  $\hat{\mathbf{y}}(t)$  is a vector of outputs from the system (6.1) and  $\mathbf{L}(t)$  is a time variant observer gain, specified as

$$\mathbf{L}(t) = \mathbf{P}_e(t)\mathbf{C}^T(t)\mathbf{R}_e^{-1} \quad (6.2)$$

with  $\mathbf{C}(t) = \frac{\partial \hat{\mathbf{y}}}{\partial \hat{\mathbf{x}}}(\hat{\mathbf{x}}(t))$ . Then for some positive-definite weights  $\mathbf{Q}_e$ ,  $\mathbf{R}_e$  and a real number  $\gamma > 0$  the update law based on the time-variant Riccati equation

$$\begin{aligned} \dot{\mathbf{P}}_e(t) = & (\mathbf{A}(t) + \gamma\mathbf{I})\mathbf{P}_e(t) + \mathbf{P}_e(t)(\mathbf{A}^T(t) + \gamma\mathbf{I}) \\ & - \mathbf{P}_e(t)\mathbf{C}^T(t)\mathbf{R}_e^{-1}\mathbf{C}(t)\mathbf{P}_e(t) + \mathbf{Q}_e, \end{aligned} \quad (6.3)$$

where  $\mathbf{A}(t) = \frac{\partial \mathbf{f}}{\partial \hat{\mathbf{x}}}(\hat{\mathbf{x}}(t))$ . Note that the equation (6.3) requires initial condition for matrix  $\mathbf{P}_e(0)$ . Usually this initial matrix needs to be adjusted large enough such that at observer startup no visible oscillations occur. The constant  $\gamma$  in the equation (6.3) serves to determine the observer error convergence (therefore the claim ‘‘prescribed degree of stability’’). In the next section the influence of this constant in the observer error dynamics will be analyzed.

## 6.2 EKF Design

Although that measurements can provide two states from three<sup>1</sup> the observer is synthetised for the whole state vector

$$\hat{\mathbf{x}} = [\hat{x}_1 \ \hat{x}_2 \ \hat{x}_3]^T. \quad (6.4)$$

---

<sup>1</sup> $p_1$  is directly measured and  $P_c$  can be inferred from (3.5)

It is done because of the presence of pressure fluctuations (detailed view in [34]) which affect the measurement as some sinusoidal noise and EKF acts as some kind optimal low-pass filter. The output vector is considered in a normalized coordinates

$$\hat{\mathbf{y}} = \begin{bmatrix} x_1 & \frac{W_c - W_c^s}{W_c^s} \end{bmatrix} \quad (6.5)$$

where  $W_c^s$  is the steady state for the measured mass flow. For given weights

$$\mathbf{Q}_e = \text{diag}(1 \ 1 \ 1), \quad \mathbf{R}_e = \text{diag}(1 \ 1) \quad (6.6)$$

the initial matrix in equation (6.3) is chosen

$$\mathbf{P}_e(0) = \text{diag}(100 \ 100 \ 100) \quad (6.7)$$

and the simulation of the observer is performed for a noisy input to watch convergence. Initial conditions for the observer are (6.8). For a comparison purpose only the third state (compressor power  $P_c$ ) is used because it has the slowest dynamics. Moreover, during the simulation a white noise is added to the outputs with maximum noise amplitude of  $10^{-2}$ . Figure 6.1 shows true  $P_c$  and estimated  $P_{ce}$  compressor power simulated with  $\gamma = 0$ . Fig. 6.2 depicts the difference between mentioned powers for rising parameter  $\gamma$ . Clearly, the speed of error dynamics grows gradually with increasing  $\gamma$ . Though faster convergence, also the sensitivity of the measurement noise is amplified. This effect is however unwanted and a compromise is needed. Therefore the EKF with  $\gamma = 0$  is chosen to recover the state.

## 6.3 Simulation Results

In this section the results obtained with employing EKF starting from miss-estimated initial values is presented. No noise is added to the outputs. Initial conditions used in the EKF regard the whole state vector and are selected to

$$\hat{\mathbf{x}}(\mathbf{0}) = (0.1 \ 0.1 \ 0.1)^T. \quad (6.8)$$

Results for IO based controller are omitted from the section because the controller does not contain an integration property. Otherwise the start point for actuator signals would

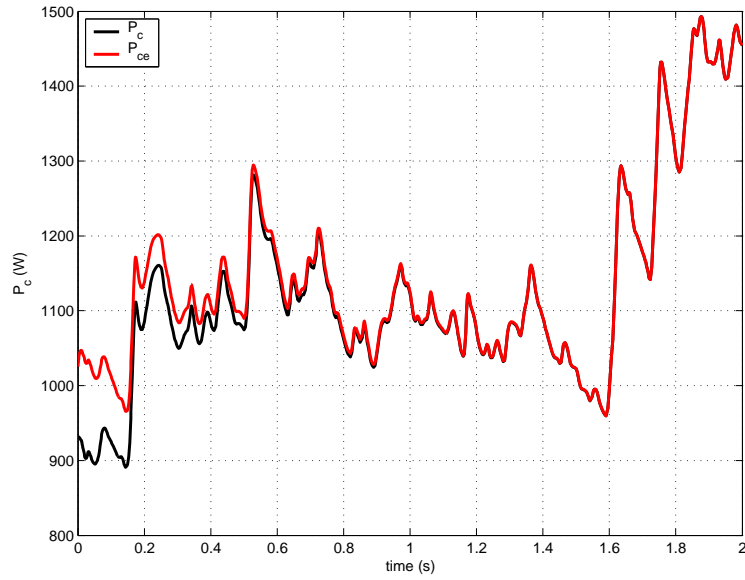
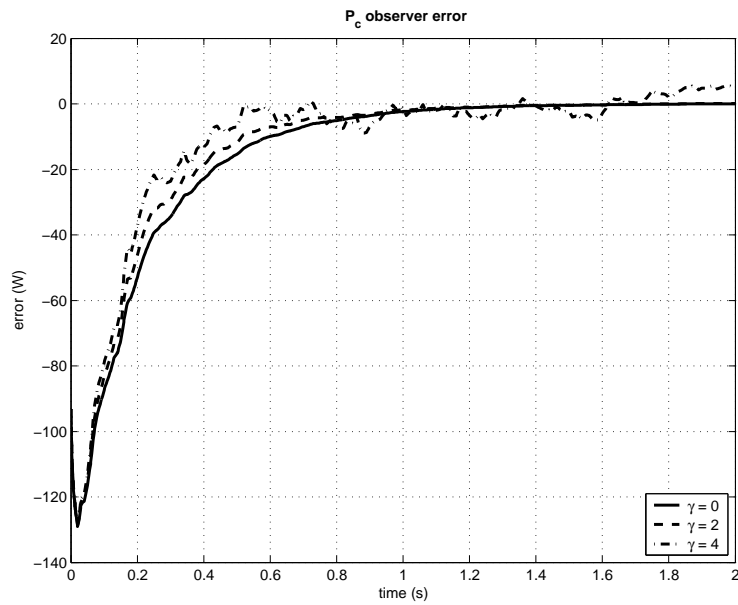


Figure 6.1: Testing the observer for a noisy input.

Figure 6.2: Increasing the parameter  $\gamma$  gains on noise sensitivity.

be affected by the initial observer error and would differ from the LQR/NMPC case where the start point is the current signal for actuator which is known as initial condition for augmented plant (5.9). In this simulation the initial conditions for the EGR/VGT were selected

$$u_1(0) = 0.1, \quad u_2(0) = 0.1. \quad (6.9)$$

In the results, only the true states are depicted. The estimated ones have been omitted, to avoid redundancy.

Figure 6.3 shows the effect of the initial observer error (6.8) for the pressure in the intake manifold. In the first second of the simulation time the pressure moves away from the desired setpoint and after the observer error disappears, the pressure approaches back to its setpoint. In Fig. 6.4 for the exhaust manifold pressure the initial observer causes a bit bigger deviation from the setpoint. This is because the exhaust manifold pressure possess faster dynamics. A difference between LQR and NMPC can be seen during the second changeover. Because the upper constraint is very close to this setpoint, NMPC accounts this limit to the stage cost and avoids closer contact. Further visible differences between LQR and NMPC are depicted in Fig. 6.7 and Fig. 6.8 where the actuator signals are plotted. The presence of constraint during the first changeover causes deviations in NMPC from the actuator setpoints. Detailed view gives Fig. 6.9 for the EGR control moves and Fig. 6.10 for the VGT control moves.

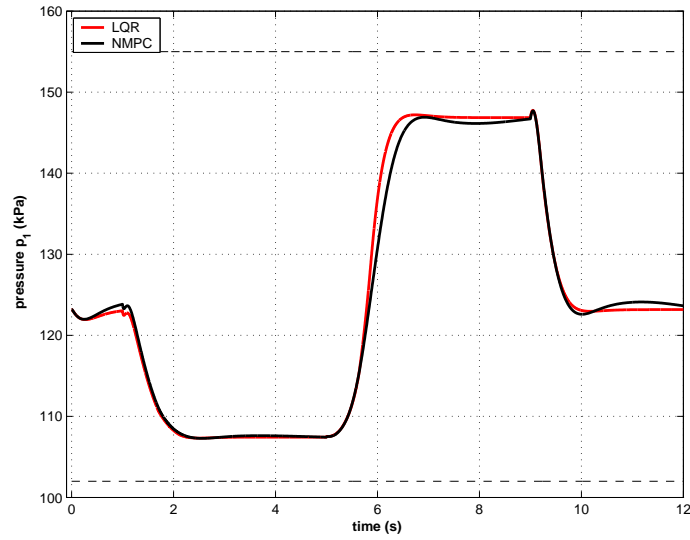


Figure 6.3: Control of the intake manifold pressure (with EKF).

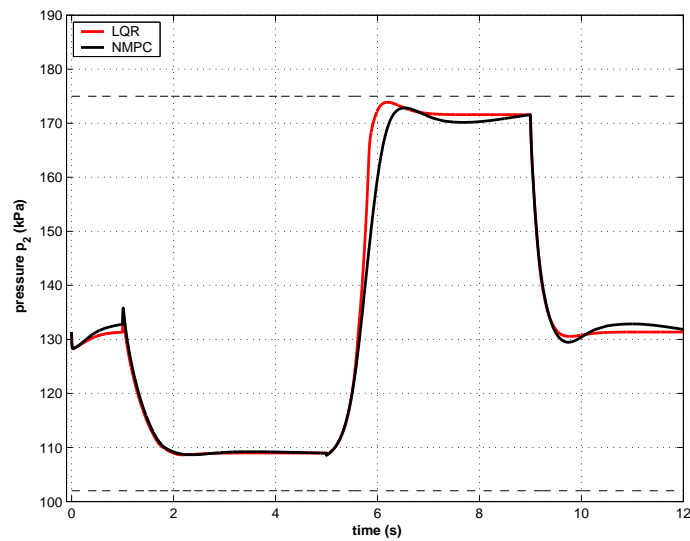


Figure 6.4: Control of the exhaust manifold pressure (with EKF).

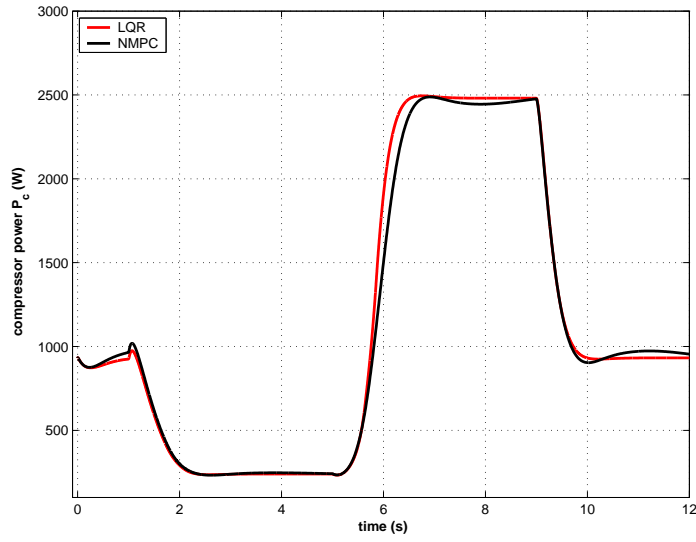


Figure 6.5: Control of the compressor power (with EKF).

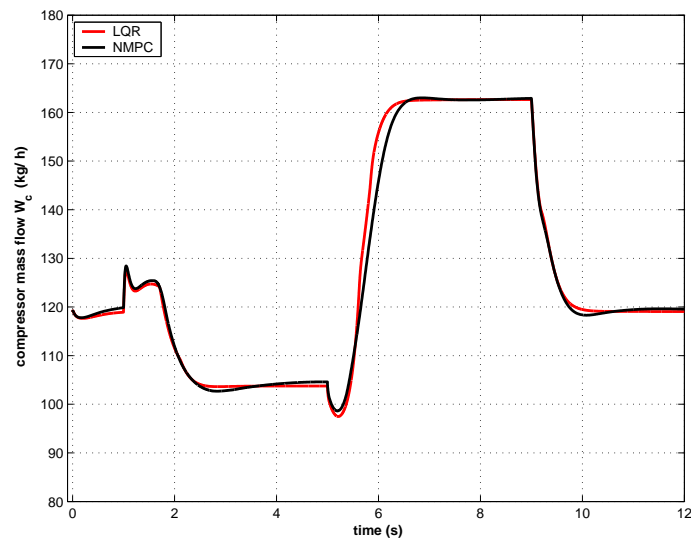


Figure 6.6: Control of the compressor mass flow (with EKF).

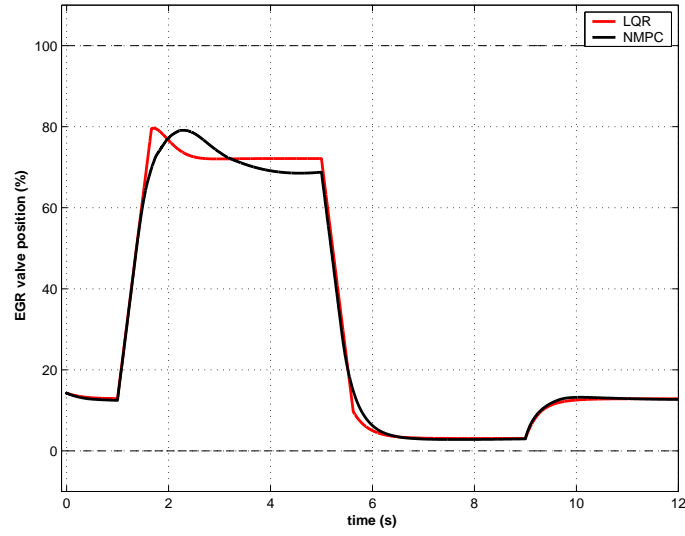


Figure 6.7: Signals for the EGR valve (with EKF).

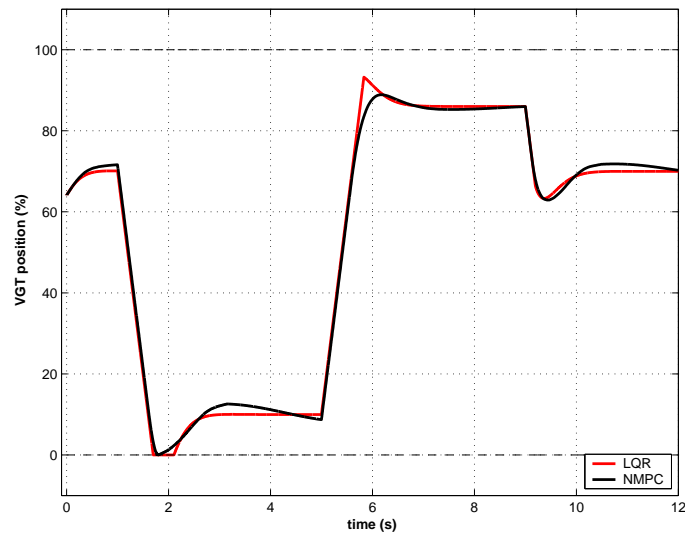


Figure 6.8: Signals for the VGT (with EKF).

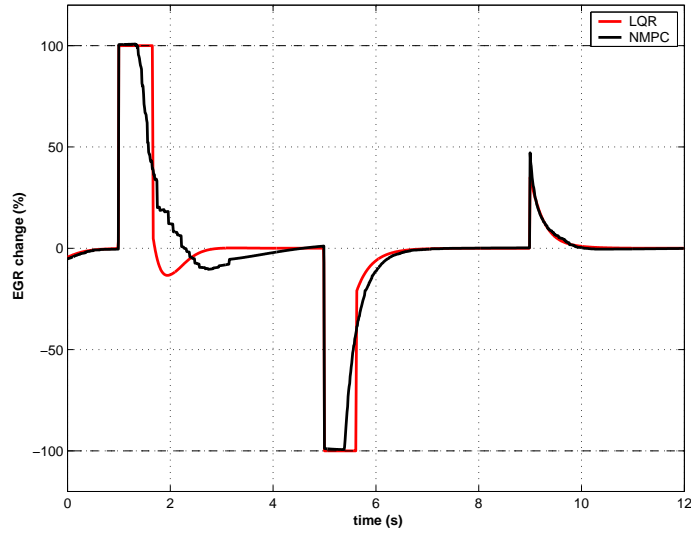


Figure 6.9: EGR control moves (with EKF).

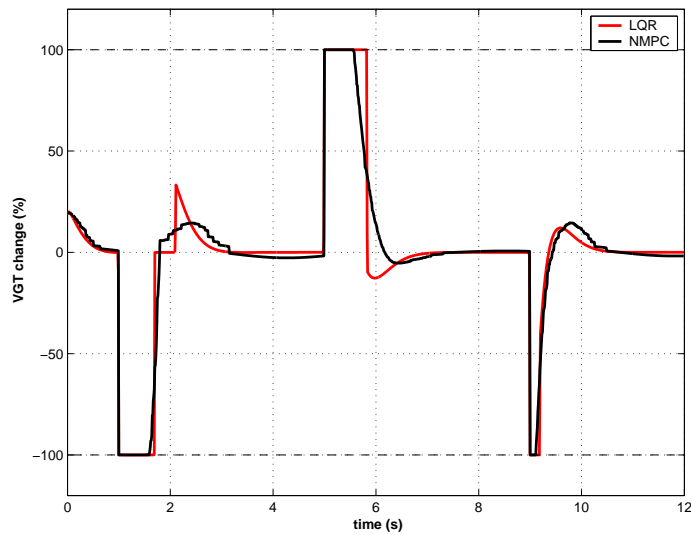


Figure 6.10: VGT control moves (with EKF).

## Chapter 7

# Conclusions

Nonlinear Model Predictive Control offers a big potentiality for controlling the diesel engine equipped with EGR and VGT. From results obtained in state feedback case or output feedback case it confirms its suitability for this control problem.

However, from the practical point of view, NMPC is not yet applicable. It is due to the computational load assigned with solving large nonlinear program. Because the sampling time is very fast, varying in milliseconds, NMPC can be only be applied in simulations. Therefore it can be considered as a benchmark for other control methods because the NMPC approach is a structural way for coping with nonlinearities and furthermore, the constraints can be treated in a more sophisticated manner.

# Bibliography

- [1] F. Allgöwer, T.A Badgewell, J.S. Qin, and S.J. Wright. Nonlinear predictive control and moving horizon estimation- an introductory overview. In *Advances in Control: Highlights of European Control Conference*, pages 391–449. Springer, 1999.
- [2] F. Allgöwer, R. Findeisen, and C. Ebenbauer. Nonlinear model predictive control. *Encyclopedia for Life Support Systems*, Article 6.43.16.2, 2004.
- [3] M. Ammann, N.P. Fekete, L. Guzella, and A.H. Glattfelder. Model-based control of VGT and EGR in a turbocharged common-rail diesel engine: theory and passenger car implementation. *Society of Automotive Engineers*, Paper 2003-01-0357, 2003.
- [4] S. Benghea, R. DeCarlo, M. Corless, and G. Rizzoni. A polytopic system approach for the hybrid control of a diesel engine using VGT/EGR. *Journal of Dynamic Systems, Measurement and Control*, 127:13–21, March 2005.
- [5] L. Biegler. Efficient solution of dynamic optimization and NMPC problems. In F. Allgöwer and A. Zheng, editors, *Nonlinear Model Predictive Control*, pages 219–244. Birkhäuser, 2000.
- [6] Christoph Böhm. Regelung eines dieselmotors. Semester thesis, Juni 2005. Institut für Systemtheory Technischer Prozesse, Universität Stuttgart.
- [7] H. Chen and F. Allgöwer. A quasi-infinity horizon nonlinear model predictive control scheme with guaranteed stability. *Automatica*, 34(10):1205–1217, 1998.

- [8] Wen-Hua Chen, John O'Reilly, and Donald J. Ballance. On attraction domain of model predictive control of nonlinear systems with input/state constraints. Technical report, Faculty of Engineering, Glasgow G12 8QQ, Scotland, 1999. Available at <http://www.mech.gla.ac.uk/Research/Control/Publications/Rabstracts/abs99009.html>.
- [9] Wen-Hua Chen, John O'Reilly, and Donald J. Ballance. On the terminal region of model predictive control for non-linear systems with input/state constraints. *International Journal of Adaptive Control and Signal Processing*, 17:195–207, 2003.
- [10] M. Čizniar, M. Fikar, and M.A Latifi. *MATLAB Dynamic Optimisation Code DYNOPT. User's Guide*. KIRP FCHPT STU, Bratislava, 2005.
- [11] G. de Nicolao, L. Magni, and R. Scattolini. Stability and robustness of nonlinear receding-horizon control. In F. Allgöwer and A. Zheng, editors, *Nonlinear Model Predictive Control*, pages 3–22. Birkhäuser, 2000.
- [12] M. Diehl, R. Findeisen, S. Schwarzkopf, I. Uslu, F. Allgöwer, H.G. Bock, and J.P Schlöder. An efficient approach for nonlinear model predictive control of large-scale systems. part I: Description of the methodology. *Automatisierungstechnik*, 12:557–567, 2002.
- [13] R. Findeisen and F. Allgöwer. An introduction to nonlinear model predictive control. In *21st Benelux Meeting on Systems and Control*, Veldhoven, Netherlands, 2002.
- [14] R. Findeisen, L. Imsland, F. Allgöwer, and B.A. Foss. State and output feedback nonlinear model predictive control:an overview. *European Journal of Control*, 9:190–206, 2003.
- [15] Rolf Findeisen, Frank Allgöwer, Moritz Diehl, H. Georg Bock, Johannes P. Schlöder, and Zoltan Nagy. Efficient nonlinear model predictive control. In *Proceedings of Chemical Process Control 6*, pages 454–460, Tuscon, Arizona, USA, 2001.

- [16] J. Fredriksson and Bo Egart. Backstepping control with local LQ performance applied to a turbocharged diesel engine. In *Proceedings of the 40th IEEE Conference on Decision and Control*, Orlando, Florida, USA, December 2001.
- [17] L. Guzella and C.H. Onder. *Introduction to Modelling and Control of Internal Combustion Engine Systems*. Springer Verlag, 2004.
- [18] M. Jankovic, M. Jankovic, and I. Kolmanovsky. Robust nonlinear controller for turbocharged diesel engine. In *Proceedings of the American Control Conference*, volume 3, pages 1389–1394, USA, 1998.
- [19] M. Jankovic, M. Jankovic, and I. Kolmanovsky. Constructive Lyapunov control design for turbocharged diesel engines. *IEEE Transactions on Control Systems Technology*, 8:288–299, 2000.
- [20] M. Jung and K. Glover. Calibratable linear parameter-varying control of turbocharged diesel engines. In *IEEE Transactions on Control Systems Technology*, volume 14, pages 45–62, 2006.
- [21] Merten Jung. *Mean-Value Modelling and Robust Control of the Airpath of a Turbocharged Diesel Engine*. PhD thesis, University of Cambridge, 2003.
- [22] Guzella L. and Amstutz A. Control of diesel engines. *Control Systems Magazine*, IEEE 18(5):53–71, Oct. 1998.
- [23] M. Larsen, M. Janković, and P.V. Kokotović. Indirect passivation design for a diesel engine model. In *Proceedings of the 2000 IEEE International Conference on Control Applications*, Anchorage, Alaska, USA, September 2000.
- [24] M. Larsen and P. Kokotović. Passivation design for a turbocharged diesel engine model. In *Proceedings of the 37th IEEE Conference on Decision and Control*, Tampa, Florida, USA, December 1998.

- [25] B. Lennox and G. Montague. Neural network control of a gasoline engine with rapid sampling. In B. Kouvaritakis and M. Cannon, editors, *Nonlinear Predictive Control*, 61. IEEE control engineering, IEEE London, 2001.
- [26] J. Löfberg. YALMIP : A toolbox for modeling and optimization in MATLAB. In *Proceedings of the CACSD Conference*, Taipei, Taiwan, 2004. Available from <http://control.ee.ethz.ch/~joloef/yalmip.php>.
- [27] D.Q. Mayne, J.B. Rawlings, C.V. Rao, and P.O.M. Scokaert. Constrained model predictive control: Stability and optimality. *Automatica*, 36:789–814, 2000.
- [28] Manfred Morari and Jay H. Lee. Model predictive control: Past, present and future. In *6th International Symposium on Process Systems Engineering and 30th European Symposium on Computer Aided Process Engineering ESCAPE-7*, Trondheim, Norway, May 1997.
- [29] S.J. Qin and T.A. Badgwell. A survey of industrial model predictive control technology. *Control engineering Practice*, 11:733–764, 2003.
- [30] J.B. Rawlings. Tutorial overview of model predictive control. *IEEE Control Systems Magazine*, 20:38–52, 2000.
- [31] K. Reif, F. Sonnemann, and R. Unbehauen. An EKF-based nonlinear observer with a prescribed degree of stability. *Automatica*, 34(9):1119–1123, 1998.
- [32] J. Rückert, F. Richert, D. Abel, O.E. Herrmann, A. Pfeifer, A. Schlosser, and S. Pischinger. A model based attempt to control boost pressure and EGR-rate for a heavy duty engine. *Automatisierungstechnik*, 53:79–86, 2005.
- [33] A.G. Stefanopoulou, I. Kolmanovsky, and J.S. Freudenberg. Control of variable geometry turbocharged diesel engines for reduced emissions. *IEEE Transactions on Control System Technology*, 8(4), July 2000.

- [34] O.F. Storset, A. Stefanopoulou, and R. Smith. Air charge estimation for turbocharged diesel engines. In *Proc. of the American Control Conference*, volume 1, pages 39–44, Chicago, Illinois, USA, 2000.
- [35] Ove F. Storset, A. Sp Stefanopoulou, and R. Smith. Adaptive air charge estimation for turbocharged diesel engines without exhaust gas recirculation. *Journal of Dynamic Systems, Measurement, and Control*, 126:633–643, September 2004.
- [36] M. van Nieuwstadt, P.E. Moraal, I.V. Kolmanovsky, A. Stefanopoulou, P. Wood, and M. Criddle. Decentralized and multivariable designs for EGR-VGT control of a diesel engine. In *Proceedings IFAC Workshop, Advances in Automotive Control*, pages 191–196, Mohican State Park, Loudenville, Ohio, USA, 1998.